MODELING THE INJECTION OF CO_2-N_2 IN GAS HYDRATES TO RECOVER METHANE USING CMG STARS

By

Shruti Oza

Dr. Shirish Patil, Advisory Committee Chair
Petroleum Engineering Department

Dr. Abhijit Dandekar, Advisory Committee Chair
Petroleum Engineering Department

Dr. Santanu Khataniar, Advisory Committee Member
Petroleum Engineering Department

Dr. Yin Zhang, Advisory Committee Member
Petroleum Engineering Department

MODELING THE INJECTION OF CO_2-N_2 IN GAS HYDRATES TO RECOVER METHANE USING CMG STARS

A

PROJECT

Presented to the Faculty

of the University of Alaska Fairbanks

in Partial Fulfillment of the Requirements

for the Degree of

MASTER OF SCIENCE

By

Shruti Oza

Petroleum Engineering

Fairbanks, AK

August 2015

Abstract

The objective of this project was to develop a reservoir simulation model using CMG STARS for gas hydrates to simulate the Ignik Sikumi#1 field trial performed by ConocoPhillips at the North Slope, Alaska in 2013. The modeling efforts were focused exclusively on the injection of CO_2-N_2 in gas hydrate deposits to recover methane after an endothermic reaction. The model was history matched with the available production data from the field trial. Sensitivity analysis on hydrate saturation, intrinsic permeability, relative permeability curves, and hydrate zone size was done to determine the impact on the production. This was followed by checking the technical feasibility of the reservoir model for a long-term production of 360 days. This study describes the details of the reservoir simulation modeling concepts for gas hydrate reservoirs using CMG STARS, the impact on the long term production profile, and challenges and development schemes for future work. The results show that appropriate gas mixture can be successfully injected into hydrate bearing reservoir. The reservoir heat exchange was favorable, mitigating concerns for well bore freezing. It can be stated that CO_2-CH_4 exchange can be accomplished in hydrate reservoir although the extent is not yet known since the production declined for long term production period during forecasting study.

Table of Contents

List of Figures

List of Tables

List of Appendices

Acknowledgments

I thank my research committee members, Dr. Shirish Patil, Dr. Abhijit Dandekar, Dr. Yin Zhang and Dr. Santanu Khataniar, for their encouragement, resource references and technical guidance through the course of my research.

I would also like to thank Kiran Venepalli and CMG STARS support team for their help with the technical details associated with using CMG STARS software for numerical modeling.

Last, but not the least, I thank all my friends and my family members. Without their unconditional love and support, I would not have accomplished this research.

Chapter 1 Introduction

1.1 Background

Energy supply and demand plays an important role in the economic development of a country. Projecting to 2015, energy consumption is expected to increase more than 50% (EIA, 2011). Organization for Economic Cooperation and Development (OECD) countries like the U.S., Europe, Japan, Korea, and others consume the most energy per capita. Energy demands in OECD countries are projected to grow annually at a slower rate of 0.9%, whereas energy consumption in non-OECD emerging economies like China and India is projected to grow at an annual rate of 2.3% due to rapid economic growth. Since the U.S. imports 60% of its crude oil demand, fluctuations in the price of crude oil have a great impact on the U.S. economy. Average annual oil price is shown in figure 1.1.

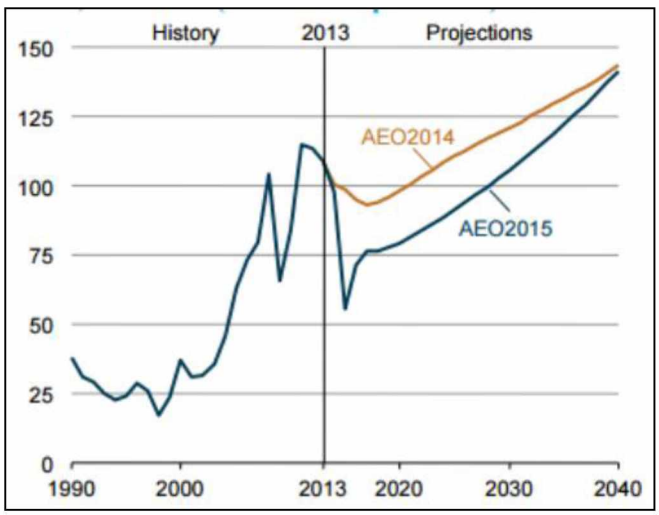

Figure 1.1 Average annual oil price (U.S. Energy Information Administration, Annual Energy Outlook 2015)

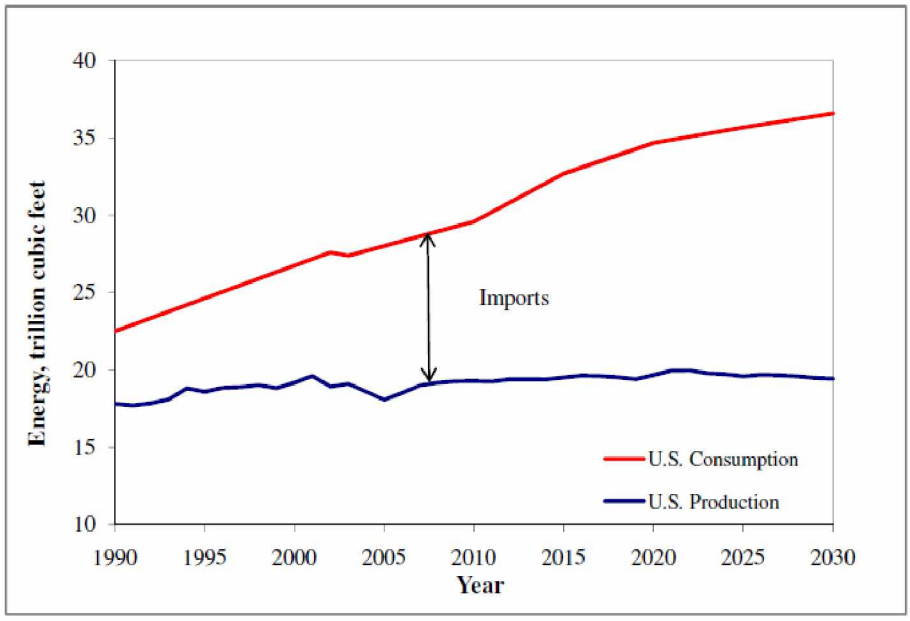

Figure 1.2 U.S. natural gas production and consumption (Gadipati, 2008)

Figure 1.2 shows the U.S consumption and production till 2030. Natural gas is the world's fastest growing fossil fuel with consumption expected to increase at an average rate of 1.6% per year from 2008 to 2030 (EIA, 2011). Because of the lower carbon emissions compared to coal and oil, natural gas is the fuel of choice in the electric power and industrial sectors in many regions of the world. In addition, it is an attractive alternative fuel for new power generation plants because of low capital costs and favorable thermal efficiencies.

In recent years, U.S. shale gas production has increased 14-fold, leading to a decline in net imports of natural gas. The high increase in natural gas production is attributed to recent advances in horizontal drilling and hydraulic fracturing technologies. The net imports of natural gas are projected to fall from 11% in 2011 to 1% in 2035 (Gadapati, 2008). This can be seen in Figure 1.3.

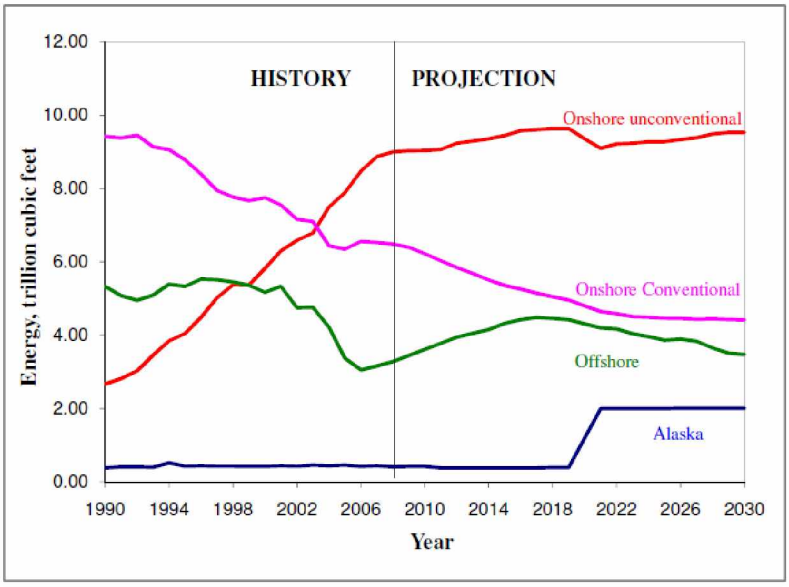

Figure 1.3 U.S. natural gas production sources (Gadapati, 2008)

Figure 1.3 also shows the onshore and offshore conventional resources show a decline from 1990 to 2030. Production of gas from onshore unconventional resources like shale gas, tight gas, and coal bed methane shows an increase when projected to 2030. Potentially, there is a vast resource of hydrate accumulations in the United States. If a fraction these hydrates could be recovered for gas production, it could address the increase in future energy demands significantly.

Natural gas hydrates are ice-like solids that do not flow, but grow rapidly and agglomerate to sizes that can block pipelines (Hammerschmidt, 1934). Gas hydrates have been a challenge in gas and oil pipelines for many decades. They are known to plug pipelines, which can cause unexpected leaks due to pipeline rupture. Hydrates can form in the pipelines' valves, lines, and elbows, among other places, whenever the pertinent temperature and pressure conditions are met. The current knowledge about hydrate occurrence in the

world is insufficient. The majority of known gas hydrate occurrences are on continental margins. Fig 1.4 shows location of gas hydrates. Current volume estimates of hydrate bound gas vary widely, from 10^{15} to 10^{18} m^3 (standard conditions) (Moridis et al., 2009) .

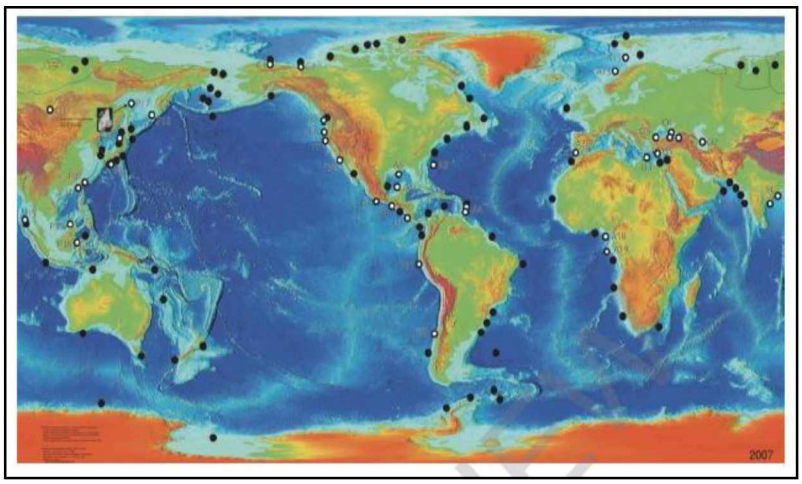

Figure 1.4 World Map showing hydrate deposits (Moridis et al., 2009)

Numerous efforts have been made recently to develop the technology to gain access to gas hydrate reserves. This study reports an enhanced recovery technique for production of gas from hydrates in an Arctic environment.

1.2 Objective

The work reported in this study was performed based on field data available from the Ignik Sikumi#1 field trial performed by ConocoPhillips at the North Slope, Alaska in 2013. The main objective of this field trial was to inject CO_2 and N_2 gas into the hydrate formation and test this potential gas hydrate production technology. The focus of this work was on developing a simulation model using CMG-STARS based on the field data from the Ignik Sikumi#1 field test. This model is validated by performing history match an sensitivity analysis. Forecasting is done on the history matched model.

The tasks performed in this study were as follows:

1. To develop a reservoir simulation model for the Ignik Sikmi#1 well using CMG STARS.
2. To match the reservoir's historical performance by performing field and well level matches.
3. To perform a sensitivity analysis for the history matched model.
4. To develop a reservoir simulation model showing future production based on the history match results.

Chapter 2 Literature Review

2.1 Gas Hydrates

Gas hydrates are crystalline compounds that occur when water forms a cage-like structure around smaller gas molecules. Here, the cage structure is termed the host and the gas molecules are referred to as guests. Hydrate formation is a possibility at any place where water exists in the vicinity of gas molecules at near freezing temperatures and elevated pressures. Gases such as methane, ethane, propane, iso- and n-butane, nitrogen, carbon dioxide, and hydrogen sulfide form hydrates in the presence of water at temperatures and pressure conditions different for each gas molecule. The hydrate formation reaction is described below (Moridis et al., 2008a)

$$g + n_H H_2O \rightarrow g * n_H H_2O \qquad (2.1)$$

Where g stands for gas and n_H is the hydration number (Moridis et al., 2008a).

Methane hydrates are of great interest because of their high potential energy value. It has been estimated that a single volumetric unit of hydrates can store approximately 164 volumetric units of natural gas at standard pressure and temperature (Yousif and Sloan, 1991).

2.2 Gas Hydrate Structure

Hydrates form due to the orientation and unusual behavior of water molecules. The water molecules act as the host and the gas molecules are guest molecules embedded in the cages of ice due to hydrogen bonding and van der Waals forces. The water molecule consists of one oxygen covalently bonded to two

hydrogen atoms at an angle between the atoms of 104.5. There are two unbonded electrons on the oxygen atom, which induce a partially negative charge on the oxygen atom due to its high electro negativity relative to the hydrogen atom. The partially induced charge results in the alignment of pairs of water molecules and a weak bond called a hydrogen bond. The water molecules line up and they can arrange themselves in different patterns such as those seen in the many crystal structures of water ice. There are many different known ice structures. Common structure is hexagonal (Stillinger, 1980).

Hydrocarbons and water form hydrates at low temperatures, with three different crystal structures (structure I, II, H) depending upon the size of the hydrocarbon. These three different crystal structures are formed by the combination of different basic cavities. The basic cavities of hydrate structures are labeled as n^m, where n is the number of edges and m is the number of faces, as shown in Figure 2.1.

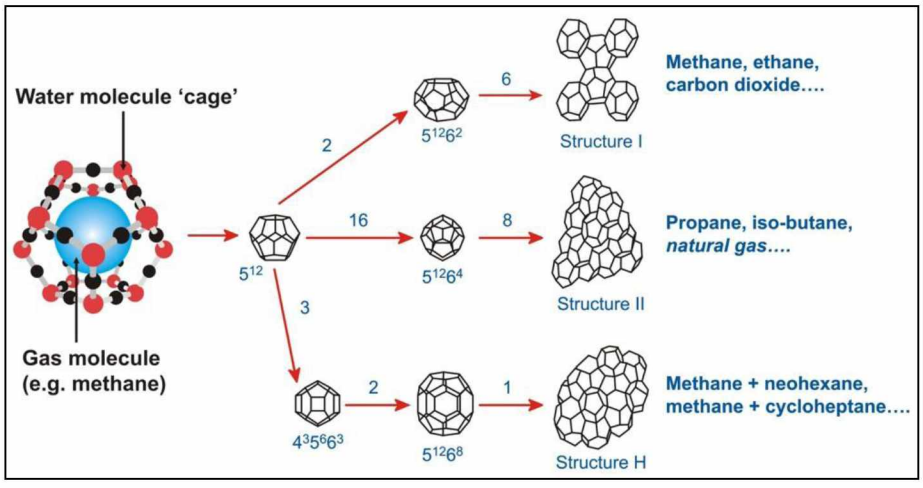

Figure 2.1 Methane Hydrate Structure (Max D., 2000)

The pentagonal dodecahedron (5^{12}) has 12 pentagonal faces with equal lengths and angles. The tetrakaidecahedron ($5^{12}\ 6^{2}$) has 12 pentagonal faces and 2 hexagonal faces and is common to SI, SII, and SH. Descriptions of different cavities like the irregular dodecahedron ($4^{3}\ 5^{6}\ 6^{3}$) are given in the table below.

Table 1 Different hydrate structure properties (Sloan, 2003)

Structure	I		II		H		
Cavity	Small	Large	Small	Large	Small	Medium	Large
Description	5^{12}	$5^{12}6^{2}$	5^{12}	$5^{12}6^{4}$	5^{12}	$4^{3}5^{6}6^{3}$	$5^{12}6^{8}$
Number of cavities/unit cell	2	6	16	8	3	2	1
Average cavity radius(Å)	3.95	4.33	3.91	4.73	3.94	4.04	5.79
Variation in radius(%)	3.4	14.4	5.5	1.73	4.0	8.5	15.1
No. of water molecules/cavity	20	24	20	28	20	20	36

1. Structure I

This structure was first observed for Ethylene oxide hydrate in 1965 by McMullan and Jeffrey (McMullan and Jeffrey, 1965). It is a face-centered cubic structure with a lattice constant of 12 Å, formed by smaller guest molecules like CH_4, C_2H_6, CO_2, and H_2S. There are 46 water molecules arranged to accommodate 8 guest molecules 4-6 Å in diameter. There are two small cages of pentagonal dodecahedra and six tetrakaidecahedra. Structural composition is $8G.46H_2O$, where G is the number of cages.

2. Structure II

Structure II was observed by McMullan and Jeffrey for a H_2S hydrate in 1965 (McMullan and Jeffrey, 1965). It is a face-centered cubic structure which can accommodate 24 guest molecules. It has 16 small and 8 large cages with 136

water molecules per unit cell. Hydrates with guest molecules like propane and iso-propane usually form this structure. The lattice constant is 17.3 A and the structural composition is $24G.136H_2O$.

3. Structure H

Structure H was first identified by Ripmeester (Ripmeester et al., 1987) in 1987. These crystals have one large cage that can accommodate big molecules like n-butane, which has a diameter of 7.1 A. Structure H is composed of three different types of cavities. It contains 34 water molecules associated with three 5^{12} cavity guest molecules, two $4^3\ 5^6\ 6^3$ cavity guest molecules and one $5^{12}\ 6^2$ cavity guest molecule. Smaller guest molecules such as CH_4, N_2, and CO_2 occupy 5^{12} cavities, and large guest molecules such as 2-methylbutane, methylcyclopentane, methylcyclo-hexane, ethylcyclohexane, and cyclooctane occupy $4^3\ 5^6\ 6^3$ cavities.

2.3 Gas Hydrate Stability Zones in Permafrost Locations

The method of identifying the zone of possible hydrate occurrence is to develop and examine the gas hydrate stability zone. The essential condition for gas hydrate stability at a given depth is that the actual Earth temperature at that depth should be lower than the equilibrium temperature of the hydrate, corresponding to existing reservoir fluid (gas) composition and pressure conditions. The thickness of a potential hydrate zone can be an important variable in a drilling operation where drilling through hydrates requires additional precautions. Thickness can also be significant in determining regions where hydrate occurrences might be sufficiently thick to justify gas recovery. The existence of a gas hydrate stability condition does not ensure

that hydrates exist in that region; however, if gas and water coexist within the hydrate stability zone, then they must exist in a gas hydrate form. Shallow hydrate reservoirs of the Alaska North Slope are good examples of hydrate accumulations associated with permafrost regions. Hydrate stability studies must be supported by physical interpretations of subsurface geology. This can be achieved by conducting core and well log evaluations and seismic surveys in order to confirm the presence of hydrates.

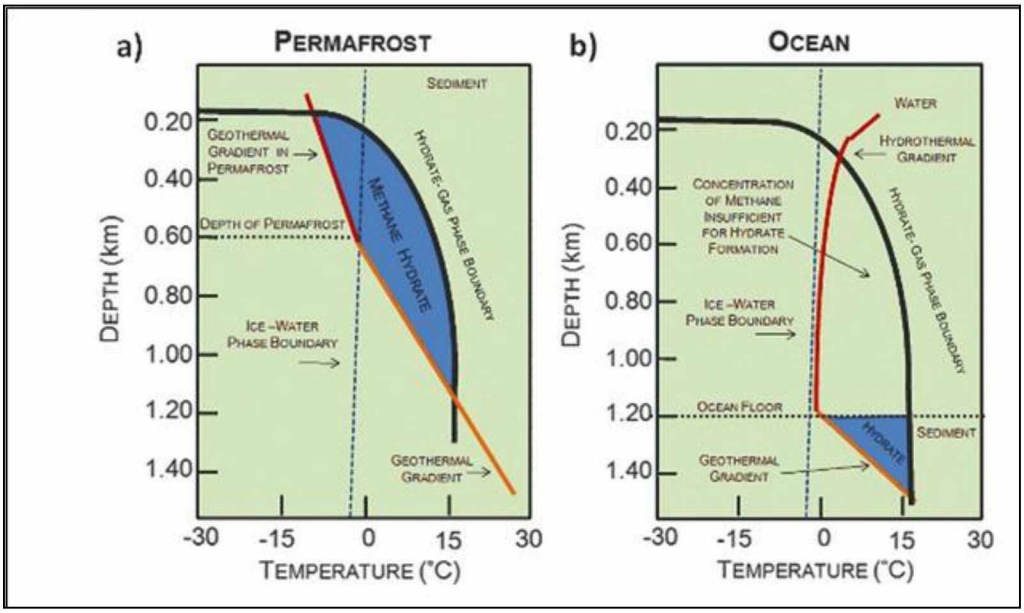

Figure 2.2 Methane hydrate stability zone (blue) for (a) permafrost and (b) oceanic environment (Moridis, 2009)

Factors affecting hydrate stability zone in the Arctic environment include (Collett et. Al., 1988):

1. Mean annual soil surface temperatures
2. Geothermal gradients within and below the base of permafrost
3. Gas composition
4. Formation water salinity
5. Reservoir rock-grain sizes
6. Subsurface pressures

Two critical factors that affect hydrate stability are gas chemistry and temperature gradient. Other factors are difficult to quantify and have little impact on hydrate stability (Collett et al., 1988).

Alaska North Slope (ANS) gas is composed mainly of methane (Collett et al., 1988), but the presence of heavier components increases the width of hydrate stability zone (Katz, 1945). On the other hand, higher water salinity tends to reduce the stability range (Sloan and Koh, 2008). Thus, it is important to collect accurate gas compositions and water salinity data for hydrate stability calculations.

Geothermal gradients have a significant impact on a hydrate stability zone (Collett et al., 1988). Permafrost regions are associated with two types of geothermal gradient: one within the permafrost region and the other below the permafrost base. Values in the ice-bearing permafrost sequence range from approximately 1.5 C/100 m in the Prudhoe Bay area to approximately 4.5 C/100 m in the east central region of the ANS. Geothermal gradients below

the ice-bearing permafrost sequence range from approximately 1.6 C/100 m to approximately 5.2 C/100 m (Collett, 1993).

2.4 Alaska Gas Hydrate Resource Potential

In 1995, the USGS conducted an assessment of the in-place natural gas hydrate resources of the U.S. (Kleinberg, 2007). The study suggested that the amount of gas in the nation's hydrate accumulations could be more than 320, 192 tcf. The USGS assessment also estimated that the permafrost-associated gas hydrates on the ANS may contain as much as 590 tcf of in-place gas (Collett, 2004). This total in place hydrates in AN is shown in figure 2.3 and figure 2.4 shows the areas of the ANS where subsurface conditions are conducive to the occurrence of gas hydrates.

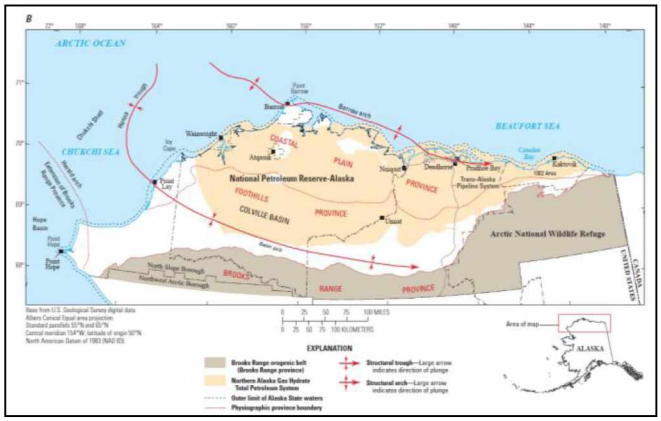

Figure 2.3 ANS Gas hydrate accumulation, (USGS 2013, modified from Collett 1993, 2002)

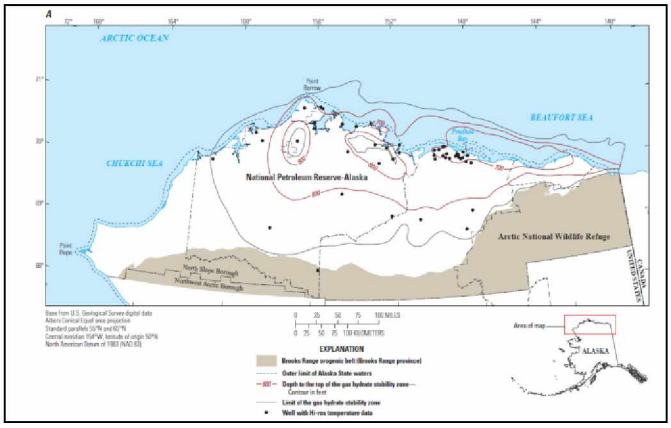

Figure 2.4 ANS gas hydrate stability zone, (USGS 2013, modified from Collett and others 1993)

2.5 Conventional Methods for Producing Gas from Gas Hydrate

The last decade has seen an increase in field-based experiments (Dallimore and Collett, 2005; Hunter et al., 2007) designed to investigate reservoir performance and well integrity issues while producing gas from hydrate-bound sediments. The majority of these field-based tests were performed in permafrost locations due to lower operating costs, better geologic information, and easier access. None of the field projects performed to date could verify the behavior of hydrate reservoirs.

Gas hydrate production schemes have been classified under three categories:

1. Thermal Injection
2. Depressurization
3. Inhibitor Injection

Gas production from hydrate involves the dissociation of in-situ hydrates. Upon dissociation, each molecule of methane hydrate produces approximately 1 molecule of methane and 6 molecules of formation water. Hence, the goal of

each scheme is to destabilize hydrates and produce gas at optimum rates such that the gas production from hydrates should cause neither uncontrolled dissociation nor re-association of produced gas and water.

The functions of these mechanisms are as follows (Darvish, 2004):

1. To bring pressure and temperature conditions of the reservoir outside the hydrate stability zone
2. To sustain the energy required for hydrate dissociation
3. To provide a means of transferring the products of decomposition to the production wells.

1. Thermal Injection

In the thermal injection method, a constant heat source in the form of steam or hot water is injected into the reservoir, causing an increase in reservoir temperature, thereby destabilizing in-situ hydrates. (Collett, 2002)

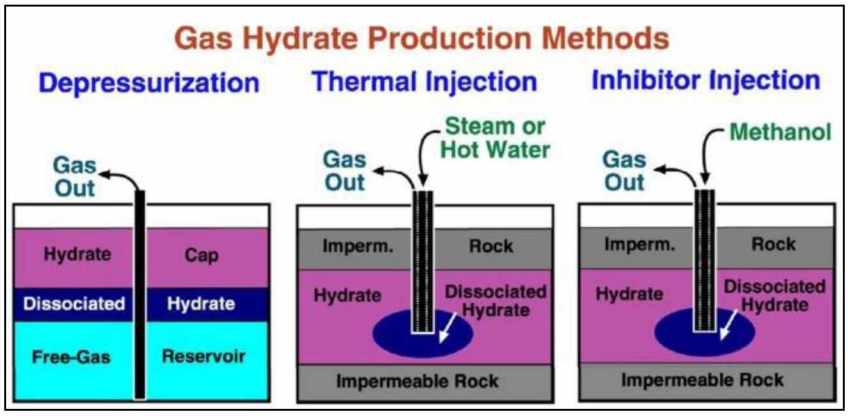

Figure 2.5 Gas hydrate production methods of depressurization, thermal injection and Inhibitor injection. (USGS Website)

The introduction of thermal energy may also be achieved by downhole processes such as in-situ combustion or electric or electromagnetic heating. The thermal injection method was applied on a field-scale during Mallik tests on the ANS in 2002. Short-term depressurization tests were followed by a thermal stimulation run which was performed by circulating warm water

through a highly concentrated gas which was produced at various rates, reaching a maximum rate of 1500 m3/day (Dallimore and Collett, 2005). Swinkles and Drenth in 2000 modeled the behavior of a hydrate-capped gas reservoir using a 3D thermal reservoir simulator. They simulated several gas production scenarios and reported good recovery using the thermal injection technique. However, the concern here was about the role of excessive water production and suggested the need for setting up water handling facilities.

The thermal injection technique has a major disadvantage: the variable cost of operation is substantially higher than that of the depressurization method. The thermal efficiency of the system needs to be monitored on a regular basis, as the chances of heat loss to the surrounding rocks are very high. This technique may not be a good option for a hydrate-bound system in permafrost locations. Long-term thermal injection could lead to heat transfer to the permafrost zone, making it unstable, thereby reducing sediment strength and integrity. Whenever desired, such a gas recovery scheme will call for careful economic evaluation and detailed engineering.

2. Depressurization

In the depressurization technique, the fluid pressure in contact with hydrates is lowered by production, thus bringing hydrates out of the stability region and causing them to dissociate. Figure 2.7 shows the depressurization pressure temperature curve.

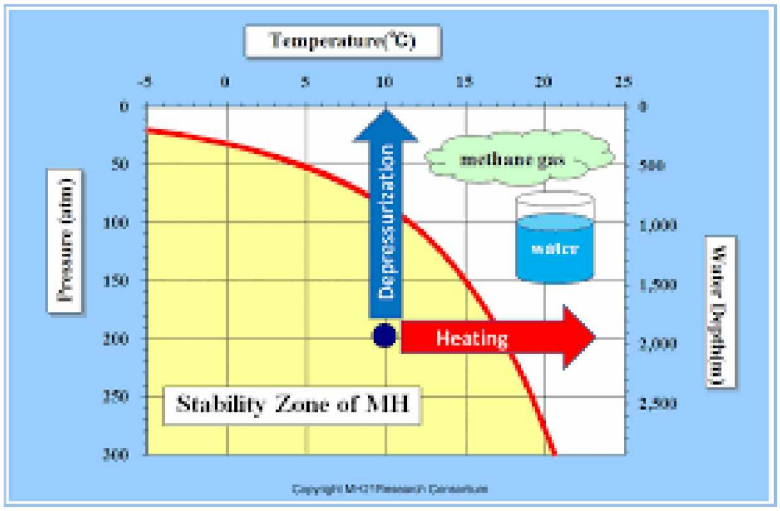

Figure 2.6 Pressure-temperature equilibrium curve showing hydrate production for depressurization (MH1 Research Consortium)

The heat required for hydrate decomposition is supplied by the surrounding rocks. The quality, type, and thermal properties of overburden and underburden rocks could play the role of rate-determining step (Selim and Sloan, 1990; Hong and Darvish, 2005). Hence, reservoirs having a larger surface area for heat transfer and hydrate decomposition would be an attractive target for gas production by depressurization. Hydrate production from depressurization is governed by three important mechanisms: fluid flow driven, kinetics driven, and heat transfer driven (Darvish, 2004).

1. Flow Driven Mechanism: Gas production reduces reservoir pressure, causing a pressure difference between the reservoir fluid (p_o) and fluid/hydrate interference (p_g).

2. Kinetics-Driven Mechanism: At constant temperature (T_s), the hydrate dissociation rate is proportional to the difference in hydrate equilibrium

pressure (p_{se}) and fluid pressure (p_g) at the fluid/hydrate interface (Kim et al., 1987).

3. Heat Transfer-Driven Mechanism: A cooling effect due to hydrate decomposition (endothermic process) causes a temperature difference between the initial hydrate temperature (T_i) and the hydrate dissociation temperature (T_s). Heat then flows from the surrounding rocks and fluids to the cooler zones. The rate of heat transfer is governed by the temperature gradient.

Studies have shown that the presence of a free gas zone right beneath the hydrate zone is the best-case scenario for gas production from hydrates (Hong, 2003; Darvish, 2004). Free gas production reduces pressure in the hydrate zone at a slower rate, thereby causing controlled dissociation of in-situ hydrates. The dissociating hydrates recharge the reservoir with additional free gas. Depressurization is the most economical of the three methods (Moridis et al., 2009). However, there are concerns that depressurization could lead to ice formation that may affect long-term production. As with other mechanisms, gas production by depressurization will generate large volumes of mobile water (Graue et al., 2006a).

3. Inhibitor Injection

Inhibitors such as methanol and calcium chloride can decompose stable hydrates by shifting the pressure-temperature equilibrium curves.

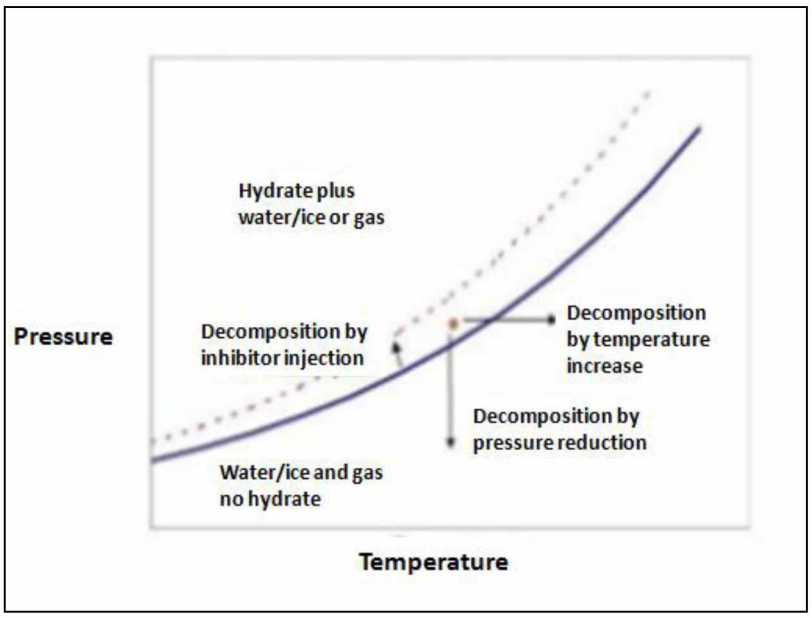

Figure 2.7 Water hydrate gas 3 phase equilibrium curve & methods of hydrate decomposition (Darvish 2004)

This method of production by inhibitor injection may not be practical at the field level due to the high cost of inhibitors and transportation of the chemicals to remote sites.

Even though the production mechanisms have been broadly classified, it should be noted that future hydrate production operations may employ a combination of these mechanisms. This will be done in order to control hydrate dissociation, minimize ice or hydrate formation, stabilize the wellbore, and maintain long-term gas production through production wells.

2.6 Types of Gas hydrate bearing reservoirs

Based on reported geologic occurrences to date, natural gas hydrate accumulations have been divided into 3 main classes, i.e., Class 1, Class 2, and Class 3 (Moridis and Collett, 2004). Class 1 accumulations are composed

of two layers: a hydrate zone and an underlying 2 phase fluid zone of free gas and liquid water.

Class 1 deposits have been subclassified into two kinds: called class 1G (water-poor system), in which hydrates and free gas exist in a hydrate zone, and class 1W (gas-poor system), in which hydrate and water exist in a hydrate layer. This class of hydrate exists when the stable hydrate zone envelope coincides with the bottom of the hydrate layer. These accumulations have been considered the most desirable distribution, as it is easier to destabilize and control hydrate dissociation by producing gas from the free gas layer (Hong, 2003; Darvish, 2004; Moridis et al., 2008a). Wells are completed in the gas zone, similar to a conventional gas well. Wellbore instability due to hydrate dissociation may remain a critical issue. The Messoyakha field in Siberia and the Barrow Gas Fields (BGF) in Alaska are good examples of class 1 hydrate accumulations (Makogon, 2009).

The second class of hydrate deposits are comprised of 2 zones, a hydrate bearing zone and an underlying aquifer (mobile water) zone. For producing gas at an economical rate from such accumulations, these reservoirs require an initial water production phase followed by a warm water injection process, or a combination of both the techniques, in order to reduce hydrate zone pressure and increase the temperature (Moridis and Reagen, 2007).

Class 3 hydrate accumulations consist of a single zone of hydrate layer. No supporting fluid zones lie beneath the hydrate zone. Lower reservoir temperatures and the absence of a supporting fluid phase limit gas production from hydrate dissociation. In reality, no single hydrate production mechanism

would be able to maintain economic rates of gas production from dissociating hydrates.

New Class 4 deposits are now being proposed, specific to hydrate accumulations found in marine sediments. Oceanic hydrate accumulations are characterized as dispersed hydrate deposits with low hydrate saturations (<10%) that lack confining geological strata (Moridis et al., 2008a).

2.7 Numerical Simulations for Gas Hydrates

Reservoir simulation is a computational method of modeling the flow of fluids in porous media over time. A reservoir simulator is built on different mathematical models that represent the petrophysical properties of a reservoir. Usually a reservoir simulator is validated by performing history matching of the data obtained from different production wells. When the reservoir simulator is validated it is used as a tool to predict future production rates, which are very important in making investment decisions. Gas hydrates are a novel field that could potentially produce large amounts of fuel for mankind, but in reality, field-scale experiments are prohibitively costly. Also, the equipment required for gas production from a hydrate well costs millions of dollars. In this scenario, the best course is to get assurance from different reservoir simulators providing motivation for simulating gas hydrates. So far, the crucial decisions about production potentials of hydrate wells have been made based on reservoir simulations.

Gas hydrate reservoirs require special production techniques due to the low reservoir temperatures. Secondary hydrate formation and ice formation could make the dissociated gas difficult to produce due to the decreasing

permeability of the reservoir due to solid formation. Hence, there are a number of problems like highly coupled heat flow, mass flow, phase transitions, and physical and chemical properties that need to be addressed for a successful reservoir model. Based on reservoir simulations, hydrate reservoirs that contain free gas are easier to produce than those with no free gas, because free gas can be easily removed from the reservoir. This causes depressurization of the reservoir and promotes hydrate dissociation. Reservoir simulators are an effective tool to determine the most suitable technique for a particular reservoir setting.

Significant efforts have been made towards modeling hydrate-bearing reservoirs in order to understand and compare their performances under different geologic conditions and production scenarios (Howe, 2004; Moridis et al., 2005; Moridis and Reagen, 2007; Ganti, 2007; Moridis et al., 2008b). Simulation studies provide the cheapest tool to quantify hydrate potential and study the impact of dissociation mechanism on a field scale. Such studies will govern future reservoir development scenarios and help optimize suitable completion techniques and well production patterns. In recent years several improvements in simulator capabilities and modeling features have taken place. The availability of new codes and revisions of existing codes have improved analysis techniques and prediction methods (Moridis et al., 2008a). Even with limited knowledge about in-situ hydrates and the physics behind their dissociation, these simulators can determine the technical feasibility of a study area and also assist in quantifying the problem and delivering possible solutions while analyzing the parameter sensitivity.

There are several numerical simulators available that have the capability to simulate the behavior of a geologic hydrate reservoir system. The most commonly used simulators are (Moridis et al., 2008a):

i. TOUGH+HYDRATE code developed by LBNL
ii. CMG-STARS code developed by Computer Modeling Group, Canada
iii. MH-21 code developed by Japan Oil Engineering Company
iv. STOMP-HYD code developed by the University of Calgary
v. UH-HYD code developed by the University of Houston

A code comparison study was initiated by USDOE (USDOE/NETL, 2007) in order to compare and validate the performance of the codes listed above. The study showed that all codes are capable of simulating the basic hydrate dissociation mechanism within the porous media. However, in the absence of reliable field data, which is the best comparison tool, the task of code validation remained incomplete (Moridis et al., 2008a).

Chapter 3 Reservoir Simulation Work

3.1 Ignik Sikumi#1, Prudhoe Bay Unit Reservoir studies

Ignik Sikumi#1 well comes in the Sagavanirktok formation. Figure 2.8 shows the log responses for the interval studied for Ignik Sikumi#1. Gamma ray (GR) (track 1) is the sand shale discrimination tool, where the hydrate bearing sand intervals are represented by the lower GR signal. The hydrate bearing intervals are identified by high resistivity (track 4 AT90), low compressional slowness values (track 5, DTCO), and separation between the conventional density and NMR porosity curves (track 6) (NETL 2013). It is clear that the D sand is capped by a shale layer on top and there is a thick shale layer between the D sand and the upper C sand.

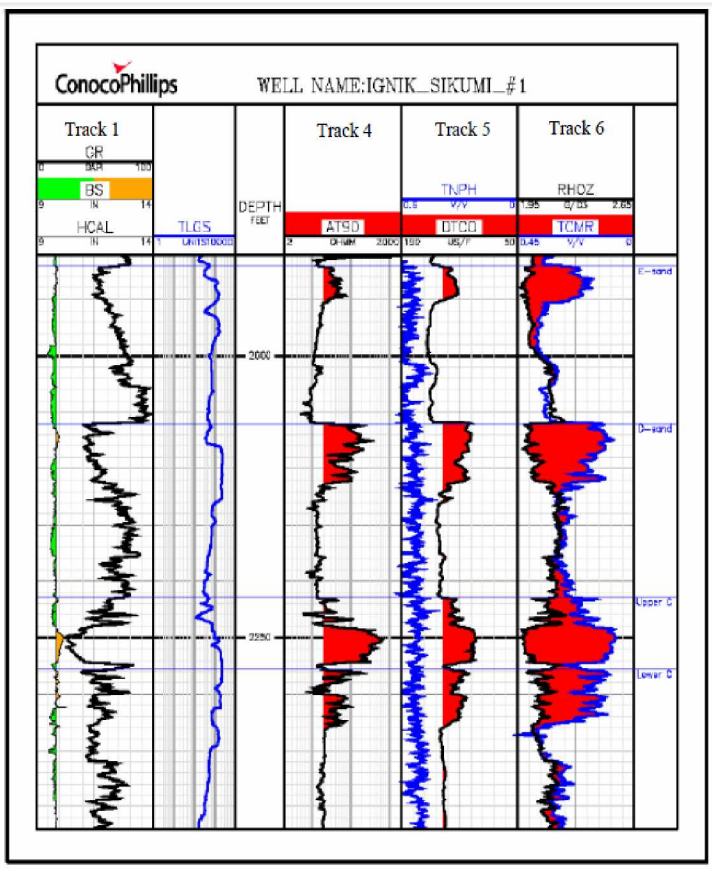

Figure 3.1 Ignik hydrate-bearing intervals shaded. (NETL 2013)

Table 2 shows the classification of sands analyzed as per the well logs.

Table 2 Sands Classification (NETL 2013)

Layers	Depth	Thickness
D Sands	628 m - 644 m / 2060ft - 2113 ft	16m (53 ft)
Shale layer	644 m - 675 m / 2113ft - 2214ft	31m (101 ft)
C (C1 Sands)	675 m - 693 m / 2214ft - 2273ft	18 m (59 ft)
Shale layer	693 m - 694.5 m / 2273ft - 2278ft	1.5 m (5 ft)
C (C2 Sands)	694 m - 719.5 m / 2278ft - 2360ft	25.5 m (82 ft)
Lower C2 - Water	710 m - 720 m / 2328ft - 2360ft	10 m (32 ft)

The Ignik Sikumi#1 test well CRA researchers used Archie's equation (Archie 1942) and Schlumberger's Density-NMR method based on a conventional gas analysis approach (Kleinberg et.al. 2005) to calculate gas hydrate saturation (S_h). Both methods provided a similar solution, with the average hydrate saturation in the upper C sands being 75%. Since neither of these methods is calibrated to cores, there is significant uncertainty in the actual saturation values.

Figure 2.9 shows the large volumes of hydrate in the upper C sand (C1)(green) and smaller amounts of free water (dark blue) and capillary bound water (light blue). The lower C sand (C2) interval below 710 m (2330 ft) contains a large volume of free water and no hydrate. The shallower D sands were not a focus of the Ignik Sikumi#1 hydrate test well.

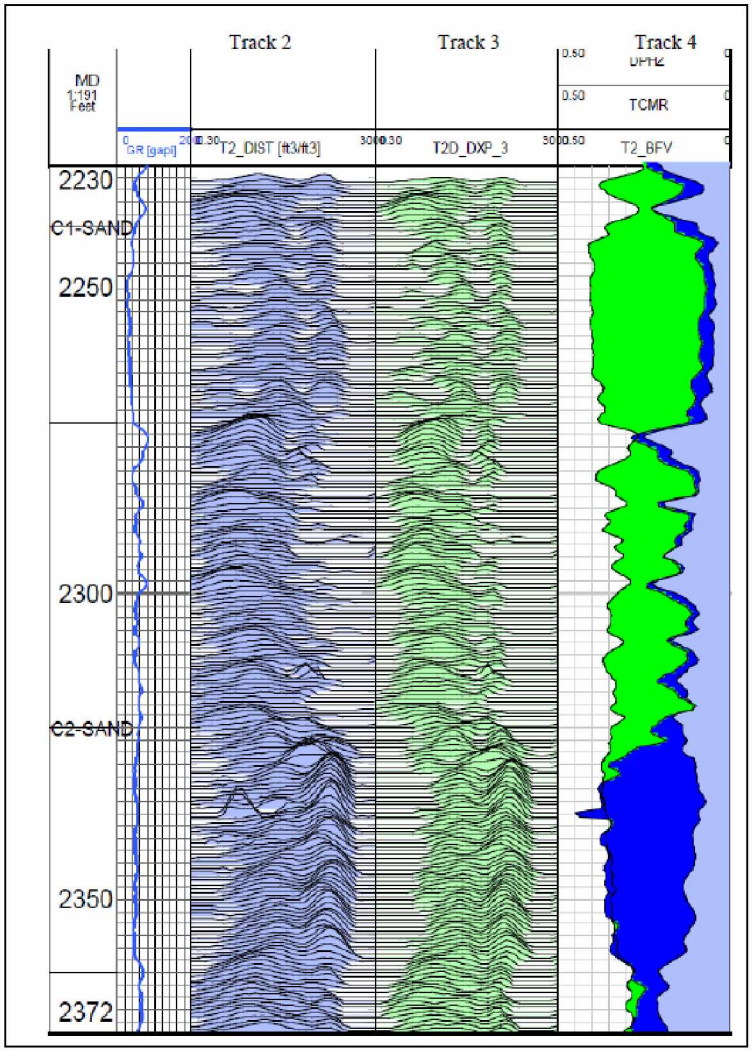

Figure 3.2 Original (track 2) and processed (track 3) NMR T2 relaxation time distributions for C sand intervals as well as hydrate and free water volume (track 4). (NETL 2013)

Track 7 of Figure 2.10 below shows the data from the XPT log. From the lower C sands (C2), below 719.5 m (2360 ft), where log results have confirmed the sands to be water saturated and devoid of gas hydrates, the intrinsic permeability is on the order of 1000 mD.

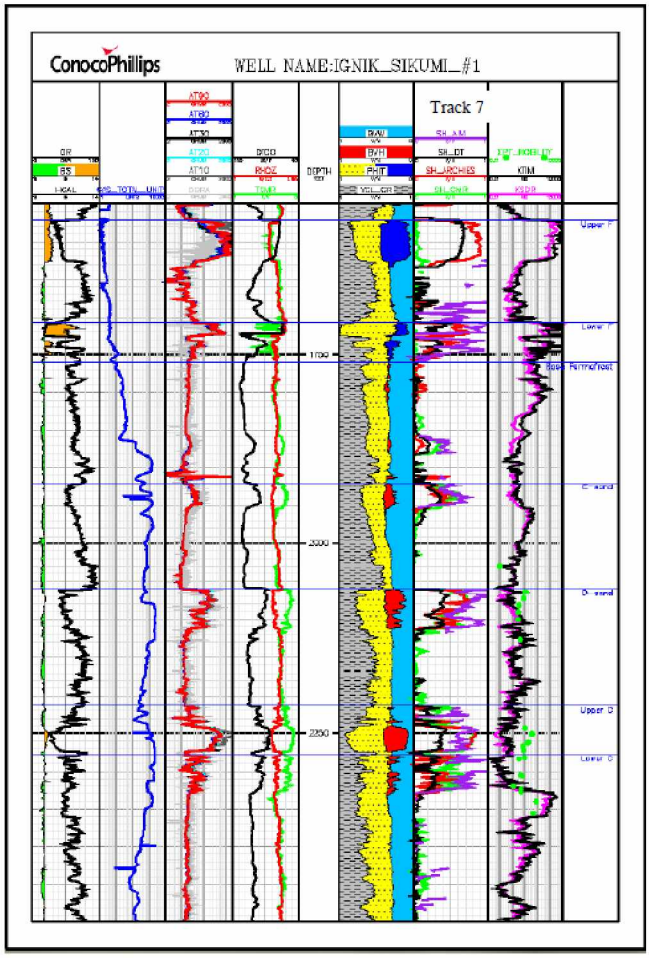

Figure 3.3 Log panel showing raw and calculated curves. Tracks from left to right: gamma ray and caliper; total gas from mud log; resistivity; neutron density and CMR; lithology; hydrate saturation and permeability with XPT mobility (NETL 2013)

The data for intrinsic permeability, hydrate saturation, porosity, and hydrate-bearing layer thickness will be used in this project to build the reservoir model.

The test design includes injection of CO_2 and nitrogen. CO_2 at surface conditions condenses to liquid at reservoir depth and temperature. Also, if excess CO_2 interacts with excess formation water, it would form additional hydrate saturation, thereby reducing permeability. For this reason, nitrogen was added in the test design as a pre-flush or as a CO_2 diluent (NETL, 2014).

3.2 Background and Objectives

Based on the Ignik Sikumi#1 wireline data, the C1 hydrate-bearing sands are thicker and higher quality than the lower C2 sands. This C1 section of the reservoir is incorporated into modeling.

CMG STARS, developed by the CMG group, was used to model gas production from a hydrate reservoir. STARS can model the flow of three-phase, multi-component fluids using Cartesian, cylindrical, or mixed coordinates. The input parameters for the model can be in the form of field data or can be generated by correlations built within the model.

For this simulation model a radial cylindrical grid was defined. It is a 4 component and 3 phase system. In CMG, hydrate can be defined as either the oil phase with very high viscosity or the solid phase. Each method has its own advantages and disadvantages. In this study, hydrate is modeled as solid.

Hydrate saturation when modeled as an oil phase represents liquid saturation. Relative permeability and capillary pressures are a function of water saturation.

$$S_l = S_w + S_h(\text{oil}) \qquad (3.1)$$

$$S_l + S_g = 1 \qquad (3.2)$$

The dependence of permeability on porosity cannot be modeled in this method.

In the case when hydrate is modeled as a solid, water and gas saturations are measured on a scale that does not include hydrate. The assumption is that hydrate is a solid and is not related to or contained in the pore spaces. The

equation used to calculate water and gas saturation is Sw + Sg = 1. Relative permeabilities in this case depend on water saturation. Hydrate properties like molecular weight, critical temperature, and critical pressure are specified in the data file. For this simulation work hydrate is modeled as a solid phase. Hydrate saturation is defined by initial solid concentration which is defined as by gmol/pore-volume. Moles of hydrate are given by,

$$moles\ of\ hydrate\ density = \frac{Sh*\rho h}{MW} \qquad (3.1)$$

Where S_h is the hydrate saturation, ρ_h is the hydrate density and MW is the molecular weight of methane hydrate.

The objectives of the simulation model are as follows:

1. To develop a reservoir model based on the Ignik Sikumi#1 well using CMG-STARS.
2. To match the reservoir's historical performance at the field and well levels.
3. To perform reservoir sensitivity analysis and compare forecasting runs and then to propose the best scenario for future production.

3.3 Base Case Model Parameters

A base case model was developed first from the Ignik Sikumi#1 test well. The following injection-production scheme was implemented on the test well. It was done in 3 phases:

1. Phase 1: Injection of CO_2/N_2 for first 14 days

2. Phase 2: Shut-in period for 5 days

3. Phase 3: Production for 30 days

Different modeling parameters were set based on the available field data and a literature review. These parameters are discussed in detail in the following section.

3.3.1 Reservoir grid

Based on reservoir geology and well log data, a base case reservoir model was generated using a radial cylindrical grid. A radial grid was selected because it is a good option to determine the sensitivity of well performance to average values of the properties. Radial grids are most accurate for vertical single well situations where flow is radial.

For this reservoir the upper C section of the reservoir (C1) was selected as the section for modeling. The upper C sand was divided into 26 layers of 0.75 m thickness. Each layer is assumed to be uniform in areal extent as far as thickness, porosity, permeability, hydrate saturation, and water saturation. A computational domain was chosen with uniform vertical spacing of 2 ft that extended over a 50-ft interval (2,234 to 2,284 ft MD). The computational domain extended radially from the well casing (0.375 ft) to an outer radial distance of 2000 ft according to the simulation work done by Anderson (Jennifer Blake, 2015). The temperature gradient for the model was entered as 1.78 F/100 ft (Jennifer Blake, 2014).

The vertical heterogeneous 3D model shown by Figure 3.1 represents upper C sand (C1) from top depth of 694 m to bottom depth of 695 m. this section is characterized by an average hydrate saturation of 75% and water saturation of 25%.

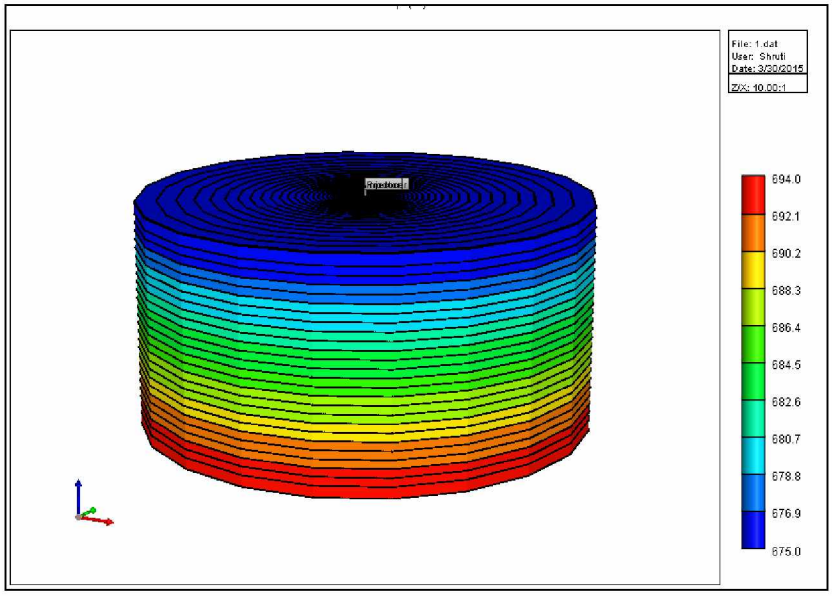

Figure 3.4 CMG STARS Radial grid for Ignik Sikumi#1

Table 3 summarizes the average properties of layers in the upper C(C1) hydrate-bearing sand for homogeneous conditions.

Table 3 Different layer properties of the C section (Jennifer Blake, 2015 & Anderson, 2014)

Reservoir Property	Value (Field Unit)	Value (SI Unit)
Reservoir thickness	50 ft	17 m
Reservoir top depth/bottom depth	2215 ft – 2265 ft	675 – 692 m
*Reservoir radial extent	2000 ft	610 m
*Total no. of layers	26	26
Reservoir pressure	1090 PSI	7500 kPa
Reservoir temperature	41 °F	5.5 °C
Porosity	0.32	0.32
*Permeability (I, j, k)	1000,1000, 100 mD	1000,1000, 100 mD
Initial solid concentration	0.28 lbmol/ft3	5500 gmol/m3
Hydrate saturation	0.75	0.75
Water saturation	0.25	0.25

3.3.2 Porosity

The porosity distribution was incorporated into the model based on the field data available in the final technical report published by ConocoPhillips to NETL (2013). The average porosity for C sands is 0.32. The geological study of the reservoir has identified the existence of semi-permeable barrier (a shale layer) at the top and bottom of C sandstone. To represent a similar condition, the top and bottom layers (layer 1 and layer 26) were assigned a lower porosity of 0.05.

3.3.3 Permeability

Estimates of permeability based on NMR measured properties were calculated with both the SDR and Timur/Coates methods (reviewed by Collett et al., 2011). Both approaches generated permeability values greater than 1000 mD in the water-bearing portion of the unit C sands, but less than 1 mD in the hydrate-bearing portion of the upper C unit sands (C1 Sand) (Anderson, 2014). The hydrate layers are assigned a permeability of 1000 mD in i and j direction and 100 mD in k direction (Blake, 2015). Figure 3.3 shows the permeability distribution within the reservoir.

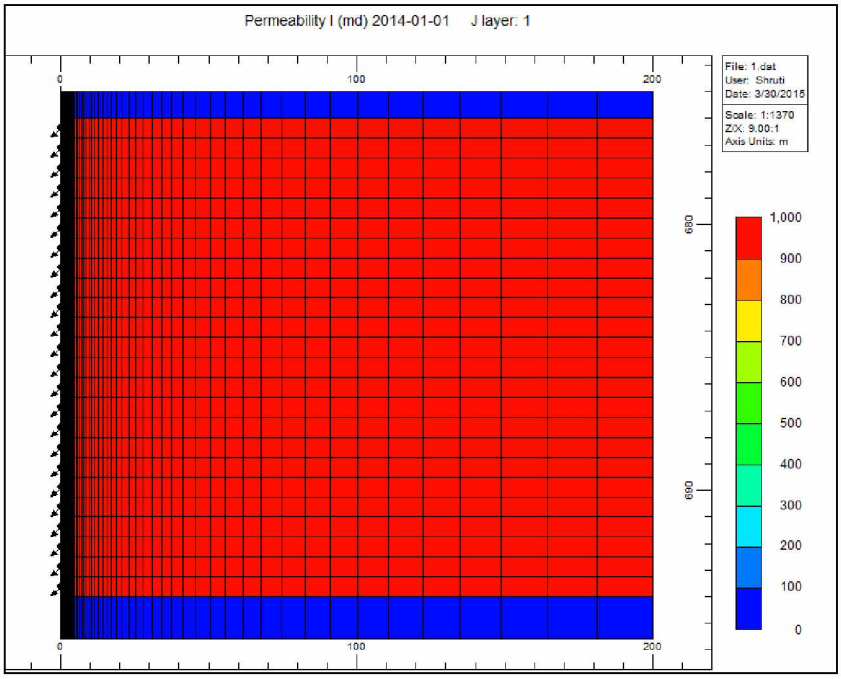

Figure 3.5 CMG-STARS model homogeneous permeability distribution

3.3.4 Initial Temperature

The geothermal gradient obtained for the PB L pad reservoir was 1.78 °F/100 ft (0.035°C/1 m). The reservoir initial temperature was 41 °F (5.5 °C) at the grid top depth. The temperature distribution within the reservoir was initialized on the basis of reservoir depth (Figure 3.3). A formula was entered in the formula editor and loaded for the model. The formula calculates the initial reservoir temperatures at respective depths.

The formula is as shown by equation 3.2, where 5 is the corresponding temperature at the grid top in °C and *X0* is the difference in top depth of the reservoir and depth at a particular layer.

$$X0 \times 0.035 + 5 \qquad (3.2)$$

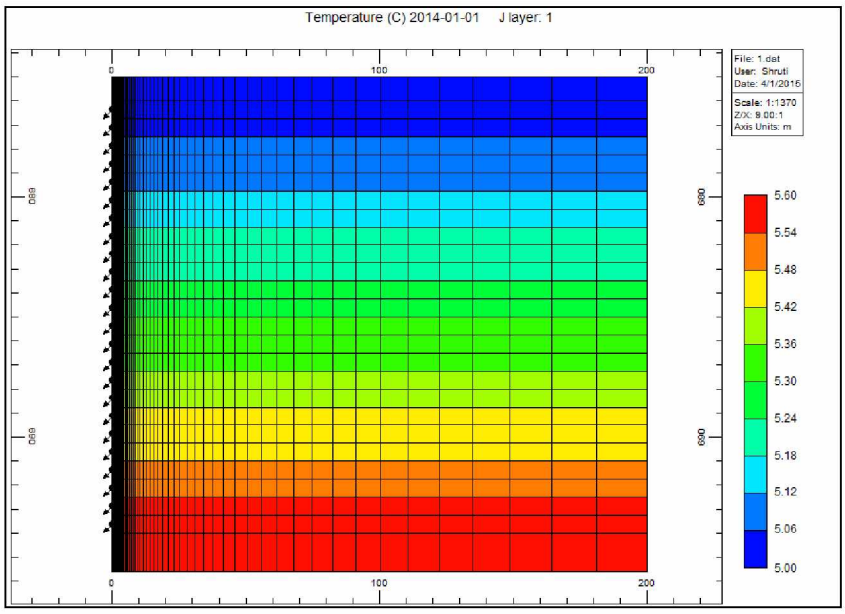

Figure 3.6 CMG STARS model temperature distribution

3.3.5 Initial reservoir pressure

Well testing and pressure gradient data reported in the final report conducted for Ignik Sikumi#1 concluded that the reservoir pressure ranged from 1075 psi to 1090 psi (NETL 2013). Pressure distribution within the reservoir is shown in figure 3.4 (Jennifer Blake, 2015).

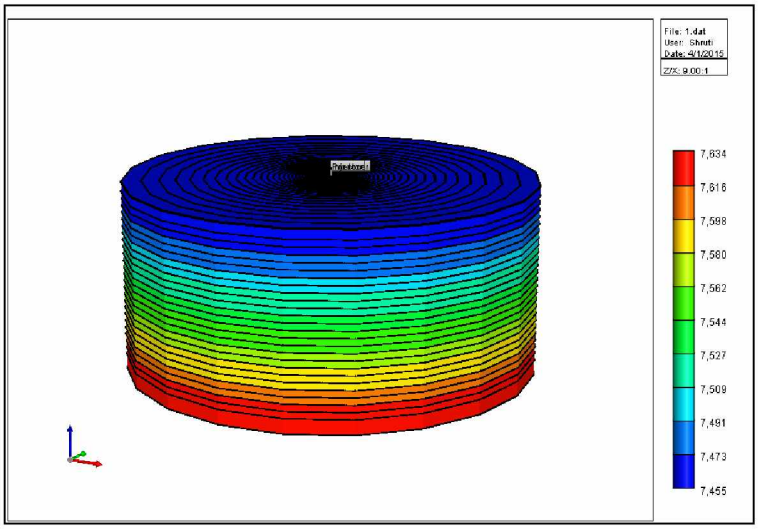

Figure 3.7 CMG STARS model pressure distribution (Jennifer Blake, 2015)

3.3.6 Components and Reactions

For hydrate gas systems, the following components were defined in CMG.

Table 4 Component system defined in CMG

Component	Phase
Methane	Gas
Water	Aqueous
CO_2	Gas
N_2	Gas
Methane Hydrate	Solid
CO_2-Hydrate	Solid

Hydrate formation and dissociation reactions are specified by equilibrium kinetics. Hydrate dissociation is an endothermic first order reaction with an enthalpy of -51857.9364J/gmol and an activation energy of 150218.3525 J/gmol (Gaddipati 2008).

$$1Hydrate = 6.1\, water + CH_4 \qquad (3.3)$$

The equilibrium (K) value for the forward and backward reactions is given by (CMG STARS):

$$K(P,T) = \left(\frac{rxk1}{P} + rxk2 \times P + rxk3\right) \times \exp\left(\frac{rxk4}{T - rxk5}\right) \qquad (3.4)$$

where *rxk1, rxk2, rxk3,rxk4* and *rxk*5 are the correlation coefficients.

Different reactions considered for this model are listed below in table 5.

Table 5 Reactions

CH_4-Hyd $\longrightarrow$ $CH_4 + 6.1H_2O$
$CH_4 + 6.1H_2O \longrightarrow CH_4$-Hyd
CO_2-Hyd $\longrightarrow$ $CO_2 + 8.7\ H_2O$
$CO_2 + 8.7H_2O \longrightarrow$ CO_2-Hyd
$CO_2 + CH_4$-Hyd $\longrightarrow$ $CH_4 + CO_2$-Hyd

3.3.7 Thermal properties

Table A1 (Appendix A) summarizes the thermal properties of rock and fluid initialized for the Ignik Sikumi#1, taken from the published work of Gaddipati (2008).

3.3.8 Fluid component properties

Table A2 (Appendix A) summarizes the fluid-component properties for the Ignik Sikumi#1 well. These properties are from Gaddipati's research (2008).

3.3.9 Relative Permeabilities

The model uses the relative permeability models of Stone (1970) and Aziz and Settari (1979). Figure 3.5 shows the Gas-Water relative permeability curve.

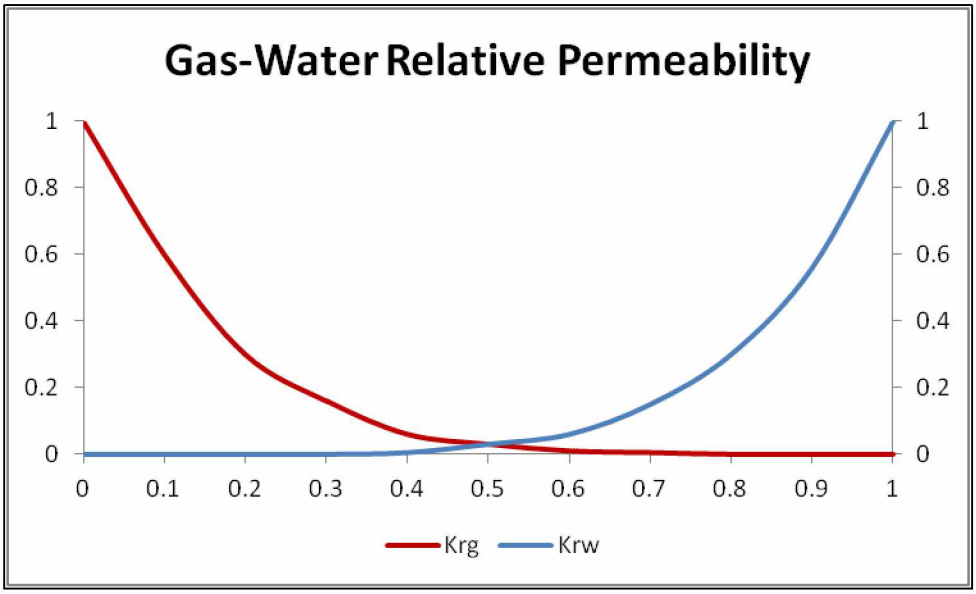

Figure 3.8 Gas-water relative permeability curves following Stone (1970)

3.4 History Match Study

The objective of the history matching analysis was to calibrate the reservoir model that closely matched the performance of the Ignik Sikumi#1 gas hydrate production and represented its reservoir conditions. While conducting the history match, availability and quality of production history, geologic, and well log data were the governing parameters.

The Ignik Sikumi#1 field has limited data. Hence, an attempt was made to develop a dynamic reservoir model that could best describe the historical performance of the reservoir.

3.4.1 Field level match criteria

Cumulative gas production obtained from the model output was compared with production history data. Pressure is a grid block property, and CMG-STARS performs material balance calculations on each grid block. Blockwise pressure data can be used to generate average reservoir pressure.

The injection rate and injection pressure in the well during the injection phase were also compared to the field data.

3.5 Sensitivity Study

The best case (history matched) was subjected to a sensitivity study. The goal of the sensitivity study was to quantify the effect of different parameters on overall reservoir performance. The following parameters were considered for the sensitivity study:

1. Hydrate saturation
2. Intrinsic permeability
3. Relative permeability
4. Hydrate zone size

3.6 Forecasting Study

A forecasting study was performed on the history match (best case) model. The CMG-STARS restart file was created to start the new simulation run from the last simulation date. For the Ignik Sikumi#1, the last simulation date was February 28, 2014. On activating the *RESTART keyword, the existing model loaded the previous simulation run obtained for the best case history matched model and started the simulation run from February 28, 2014 to February 28, 2015. For optimizing, Ignik Sikumi#1 was treated as an injection and a production well in phases. In total, 4 cycles of injection and production were considered. Each cycle was the same as the field test design.

3.7 Recovery Factor Calculation

The objective of this study was to determine the recovery factor of the field based on the performance of the field trial after the history match. After one year of operation, the increment in the recovery factor was calculated. Since original gas in place (OGIP) data was not available for the field, an OGIP calculation was done based on the dimensions of the reservoir model. The size of the base model assumed for this study was huge, with a radial stretch of 2000 ft. Hence, it should be noted that value for the recovery factor can change with variations in reservoir size. The other main assumption made during the calculation of the recovery factor was that the volume of gas hydrate in the reservoir was converted to gas volume by multiplying it by the equivalent gas hydrate volume factor of 164. Assuming that every ft^3 of hydrate in the reservoir is equivalent to 164 ft^3 of methane gas, the volumetric calculation of original gas in place was done using the following equation:

$$G(t) = \frac{V_b \phi (1 - S_w)}{B_g} \qquad (3.5)$$

Where V_b is the bulk reservoir volume in ft^3, ϕ is the porosity, S_w is the water saturation, and B_g is the gas formation volume factor. The z factor was calculated using the Hall-Yarborough correlation to obtain gas properties (Hall, K.R. and Yarborough, L. 1973). The recovery factor for the field test was then calculated as follows:

$$\text{RF} = \frac{\text{Cumulative Gas Produced in time t}}{\text{Initial Gas in Place in Hydrate form,G(t)}} \qquad (3.6)$$

Chapter 4 Results and Discussion

The CMG-STARS hydrate simulation model considers the following processes associated with hydrates:

1. Formation of hydrates
2. Dissociation of hydrates
3. Exchange of the guest molecules (CO_2/N_2)

Some of the major factors that controls the rate of hydrate formation and dissociation are the kinetic rate constants, the hydrate surface area, and the pressure differential force. The hydrate dissociation rate is also limited by the total hydrate mass present in the grid cell and the time step, such that no more than the available hydrate mass can dissociate in a single time step (Mark White, 2014).

The main objective of this project was to provide an interpretation of the available data collected from the Ignik Sikumi#1 field test. The results and analysis are explained individually for the following cases:

1. Base Case
2. History Match
3. Sensitivity Analysis
4. Forecasting Study
5. Recovery Factor

It should be noted that a lot of results are explained using the reservoir model obtained in CMG 3D results and CMG result graphs. The orientation and transition of 3D images are shown in figures 4.1 and 4.2 below.

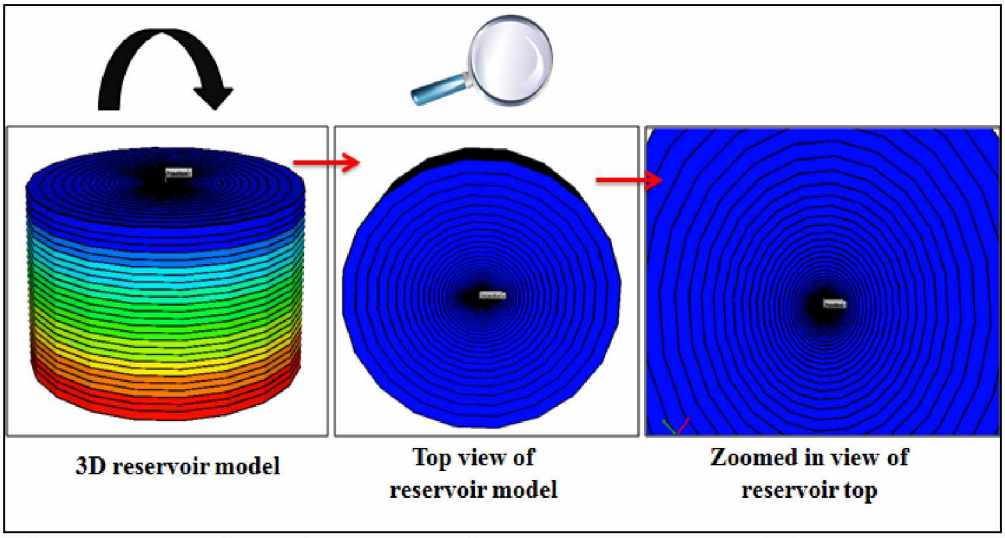

Figure 4.1 Transition showing top view of the reservoir and focusing on near wellbore area

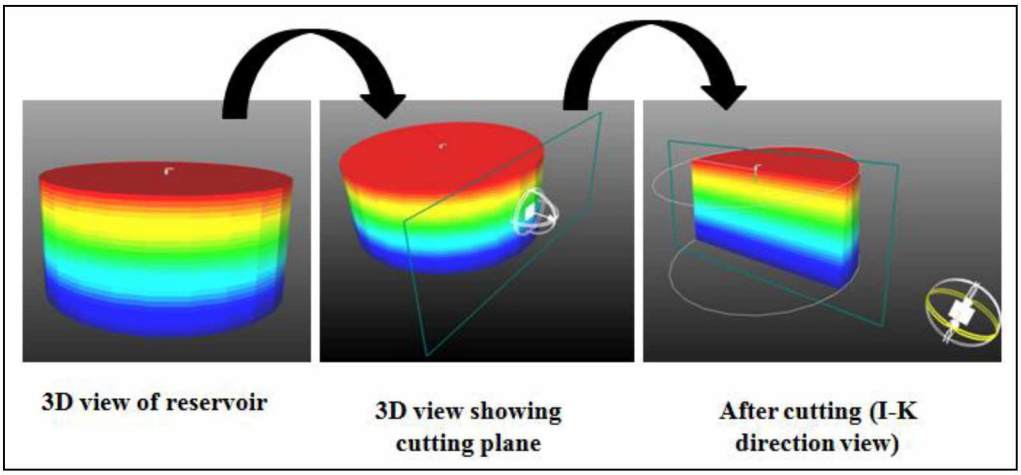

Figure 4.2 Transition showing I-K section view of the reservoir after applying cutting plane

4.1 Base Case

For the base case, CO_2 and N_2 gases were injected in a ratio of 22.5:77.5, as designed for the field trial on North Slope is shown in Figure 4.3. It can be observed from figure 4.3 that a total of 48 Mscf of CO_2 and around 170 Mscf of N_2 was injected. Figure 4.4 compares the injected amount of gases in the model to the gas injected on field.

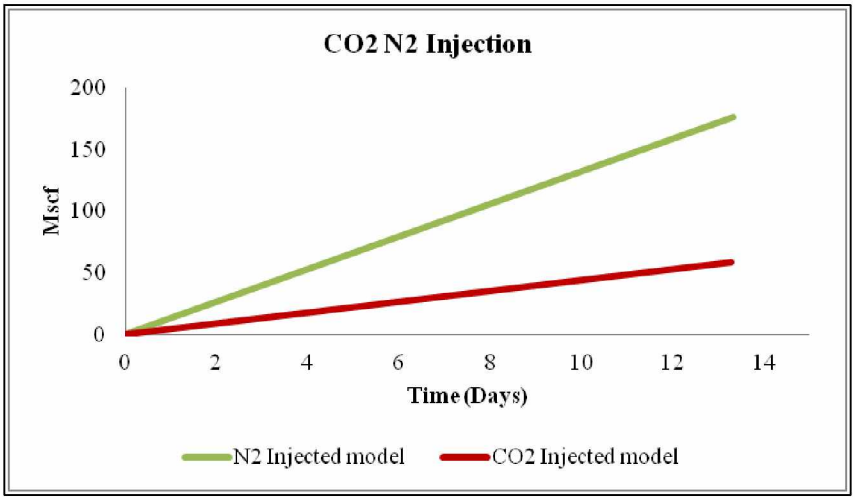

Figure 4.3 CMG STARS base case model showing injection gas ratio

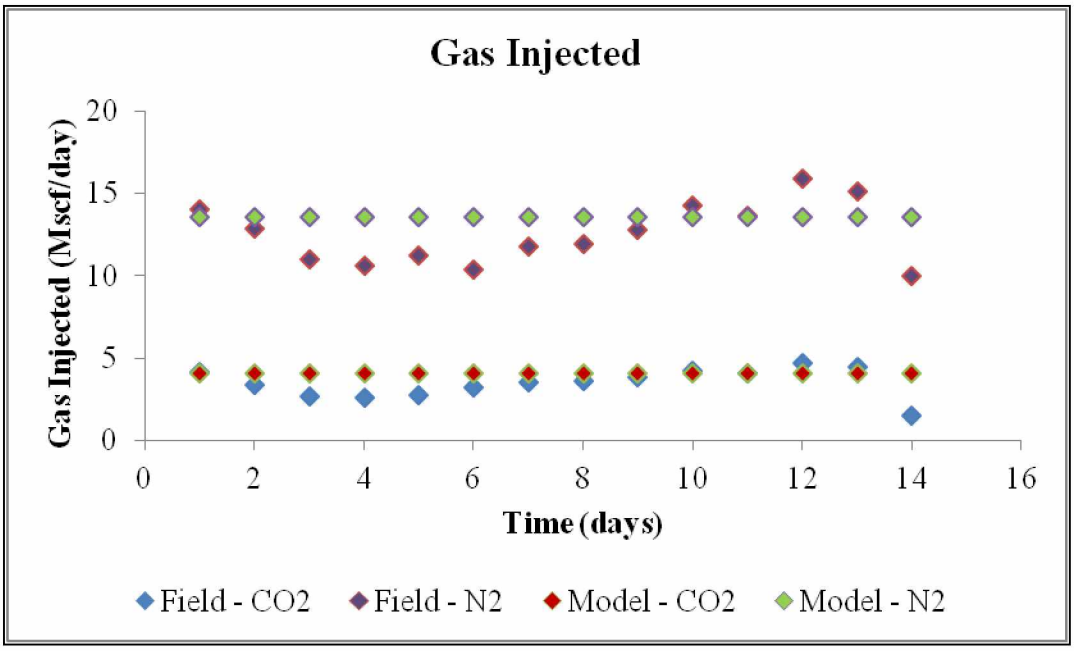

Figure 4.4 Injected CO_2, N_2 and total mixture injection for the base case model

The total injection gas rate in the model was kept constant as 500 m3/day (17.65 Mscf/day). The total CO_2 and N_2 gas injected per day in the model was around 4 Mscf/day and 14 Mscf/day. It can be observed that the injected gas in model nearly matches the field data. Figure 4.5 shows CO_2 gas mole fraction in the reservoir at the start at the end of injection phase. It can be observed that

it increased from 0 to 0.4 which reflects that CO_2 is entering the hydrate formation.

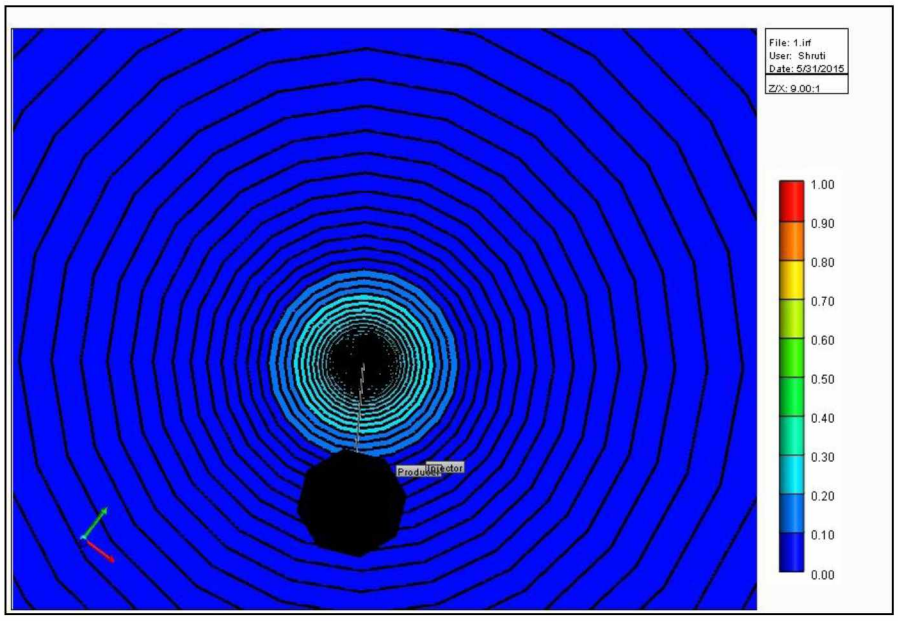

Figure 4.5 CMG STARS base case model showing CO_2 gas distribution in the reservoir at the end of injection phase.

When CO_2 is injected into a reservoir, it could react with residual water in the pores and form CO_2 hydrate. Formation of CO_2 hydrate is an exothermic reaction that will generate heat that may lead to melting of methane hydrate (Kvamme, 2012). This may happen because the generated heat from CO_2 hydrate formation (-57.98 kJ/mole) is greater than the heat required to dissociate CH_4 hydrate (54.49 kJ/mole) (Nago and Nieto, 2011). This implies that the exchange process could be a result of dissociation and reformation of hydrates. The exchange process is explained in figure 4.6.

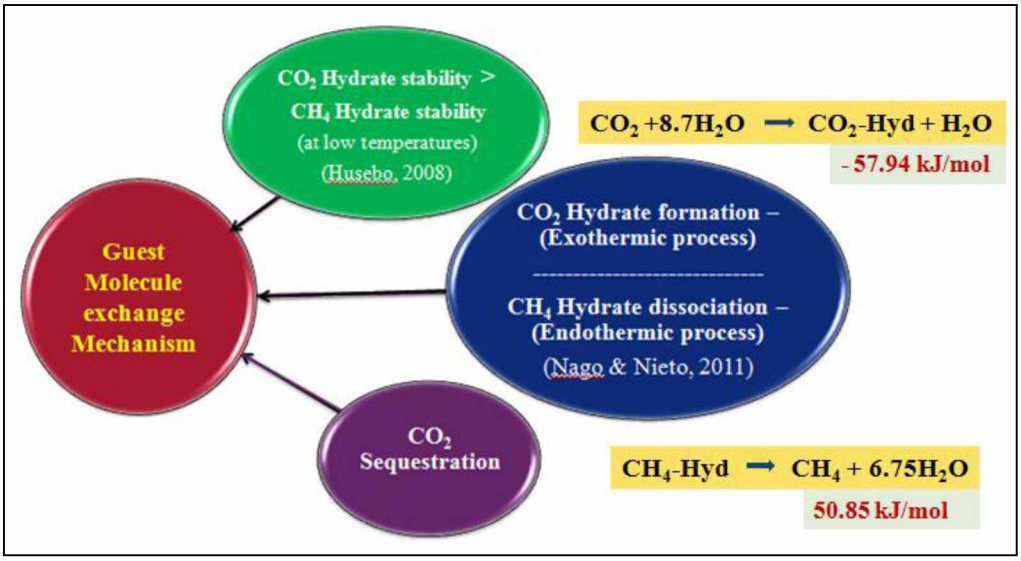

Figure 4.6 CO_2-CH_4 exchange process and reactions

As CO_2 exchanges with the CH_4 in the hydrate, the hydrate composition shifts, as does its equilibrium pressure, density, and enthalpy. The injection rate forces the gas mixture deeper into the formation, transporting unexchanged CO_2 and exchanged CH_4 away from the well. Gas migration is controlled by the heterogeneity that develops as the hydrate dissociates and forms in response to the gas mixture injection (Anderson, 2014). Figure 4.7 shows the reservoir performance of the base case at the end of production period. It can be observed that total 630 Mscf of CH_4 gas is produced along with 115 Mscf of N_2 and 7 Mscf of CO_2. As it can be observed from figure 4.7, most of the CO_2 gas is sequestered in the formation. The reason for this could be the formation of stable CO_2-Hydrates in the reservoir. CO_2 forms more stable hydrates compared to CH_4 at the temperature conditions of less than 10 C (Husebo, 2008). Since the reservoir temperature is below 10 C there is a possibility of CO_2 being sequestered as hydrate causing low recovery of CO_2 at the surface.

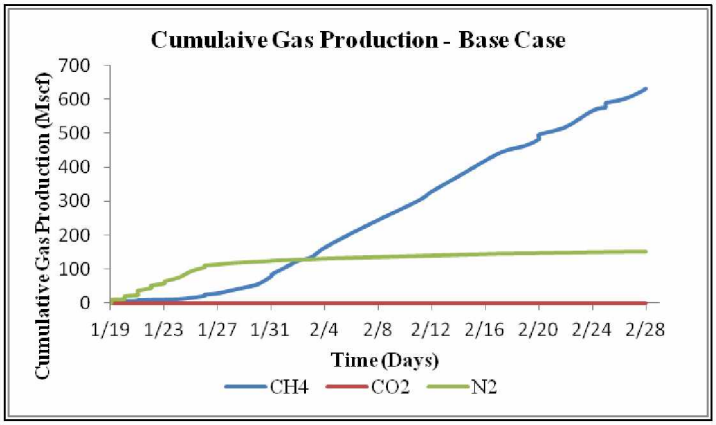

Figure 4.7 CMG base case cumulative production of CH_4 gas, CO_2 and N_2 during the production phase

4.2 History Match

After analyzing the base case, a preliminary history match study was initiated to match the base case performance to the field data. This section discusses the results obtained during the field trial as obtained from the NETL excel database. Figures 4.8, 4.9, and 4.10 show the cumulative production of CH_4, CO_2, and N_2 during the field test.

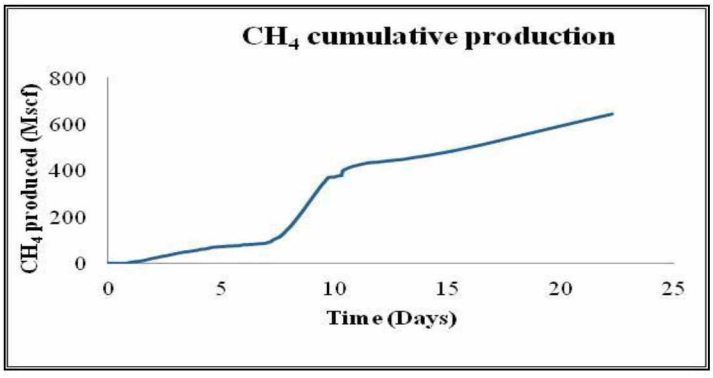

Figure 4.8 Field cumulative CH_4 production (NETL, 2014)

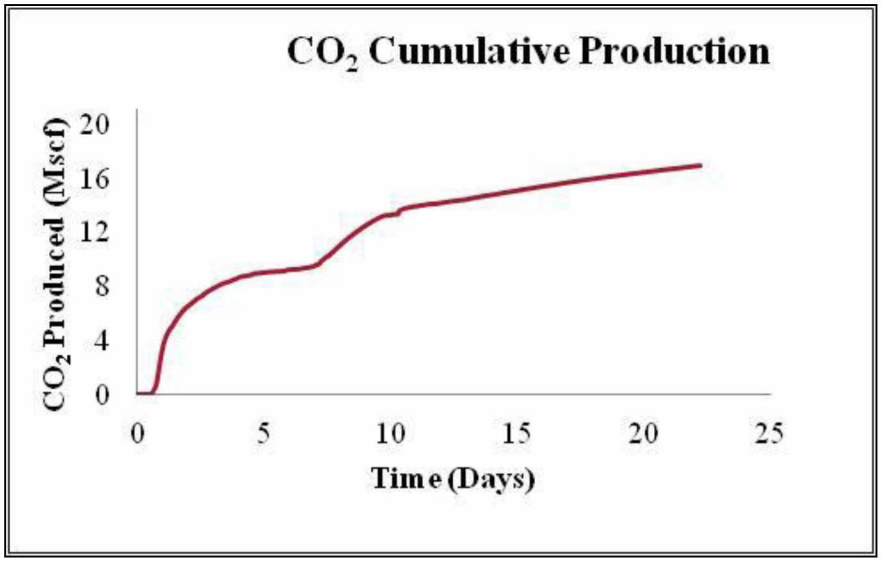

Figure 4.9 Field cumulative CO_2 production (NETL, 2014)

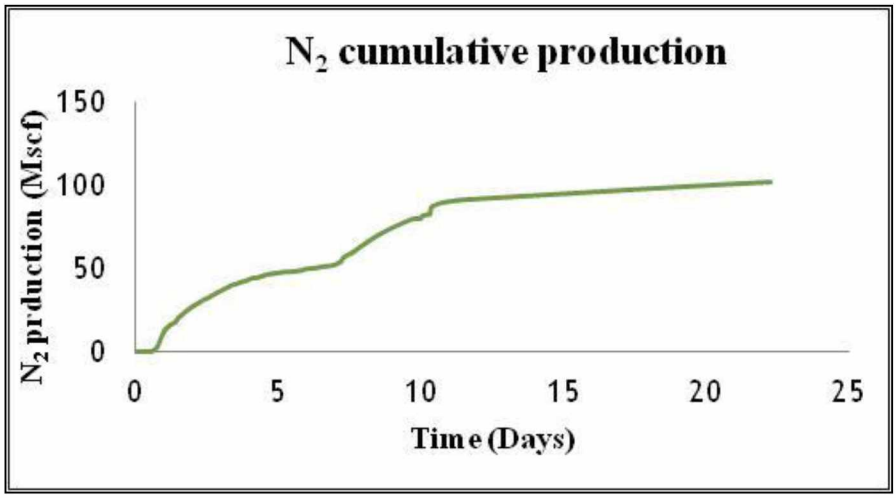

Figure 4.10 Field cumulative N_2 production (NETL, 2014)

It can be observed that a total of 755 Mscf of CH_4 gas is produced along with 110 Mscf of N_2 and 18 Mscf of CO_2 during the field trial. Table 6 shows the comparison of the base case cumulative production to the field data.

Table 6 Field and base case result comparison

Parameter	Field Value	Model Value	Error%
Cumulative CH_4 produced	855 Mscf	~650 Mscf	23.9%
Cumulative CO_2 produced	19.44 Mscf	~7 Mscf	60%
Cumulative N_2 produced	117.11 Mscf	~120 Mscf	2.4%
Cumulative Gas production	991.55 Mscf	777 Mscf	21.64%

In order to reduce the percentage error between the field data and model data of the cumulative gas production value, history matching was done by tuning the following parameters:

1. Injection/Production Bottom Hole Pressure (BHP)
2. Injection/Production Gas Rates

1. Injection/Production BHP

Figure 4.11, 4.12, and 4.13 shows the BHP during all three phases, namely injection, soak, and production, obtained from the field data.

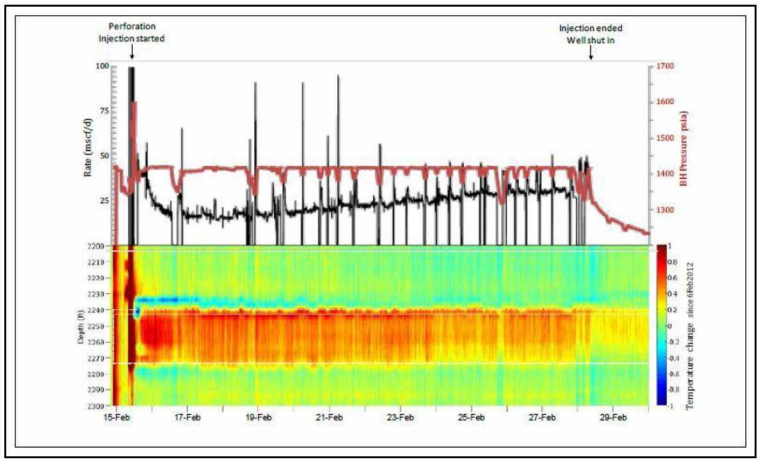

Figure 4.11 Injection phase BHP (NETL, 2014)

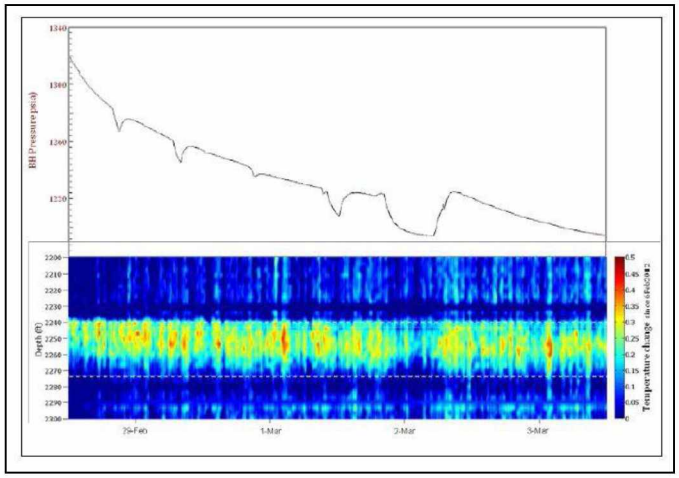

Figure 4.12 Shut-in phase BHP (NETL, 2014)

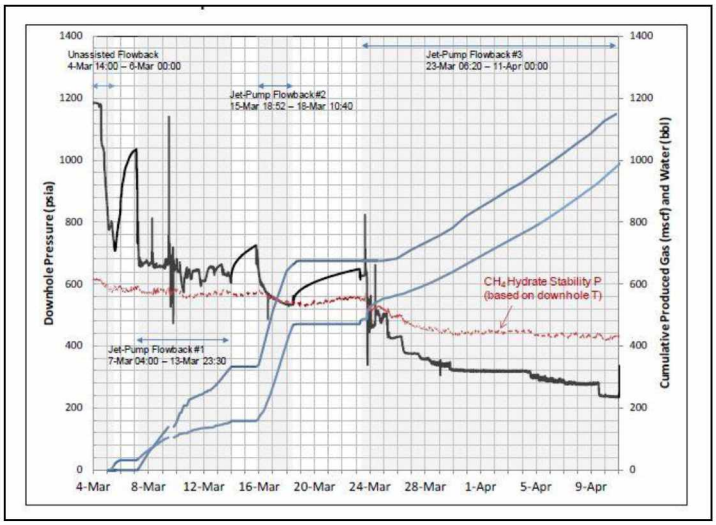

Figure 4.13 Production phase BHP (NETL, 2014)

The BHP during injection was maintained almost constant around 1400 psi, which is just below the breakdown pressure of the reservoir which is 1450 psi (NETL, 2014). During the soak period, the BHP dropped down, as expected, to 1200 psi. During the final stage of production, the pressure dropped further from 1200 to 200 psi. Figure 4.13 shows that in the first half of production, the BHP was above the hydrate stability zone. This suggests that all the gas

produced in the first half was due to CO_2/N_2 exchange and not dissociation of in-place hydrate (Anderson, 2014).

The base case injection/production well BHP was matched with the model with the help of Well Head Pressure (WHP) data available from the field excel database. In the CMG builder well and recurrent sections, different WHP values were entered from the field data files which in turn calculated the BHP. Appendix B shows the tubing table entered. Figure 4.14 and 4.15 shows the BHP distribution after history matching.

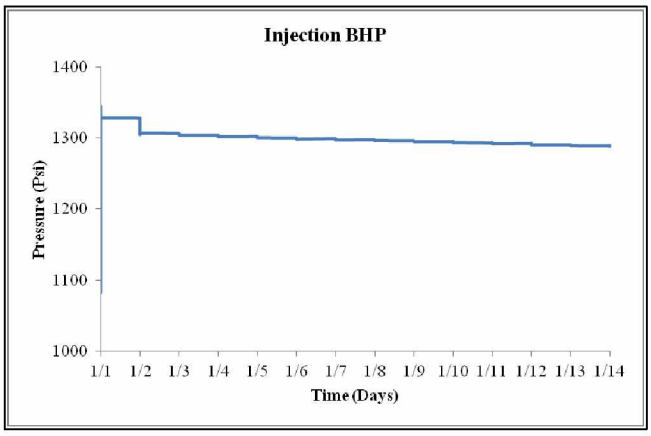

Figure 4.14 CMG model (after base case history match) result showing well bottomhole pressure during injection phase as 1300 psi.

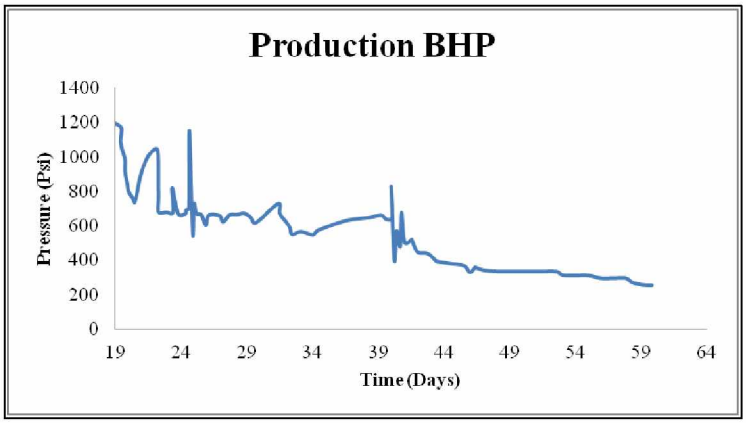

Figure 4.15 CMG model (after base case history match) plot showing model well bottomhole pressure during production phase. It shows pressure declining from 1200 psi to 200 psi.

2. Production Gas Rates

It was also observed from the field data that the production phase was divided into 3 stages separated by shut-in periods. In the first production stage the average gas production rate was of 38 Mscf/day which was followed by a 2 day shut-in period. In the second production stage the average gas production rate was 160 Mscf/day which was again followed by a shut-in period of 3 days. The third production stage had an average production rate of 300 Mscf/day. Considering these important aspects, the simulator's well production data was altered by entering the gas rate constraint for the producer well.

Figures 4.16 to 4.17 show the cumulative gas production after the history match and comparison with the field results.

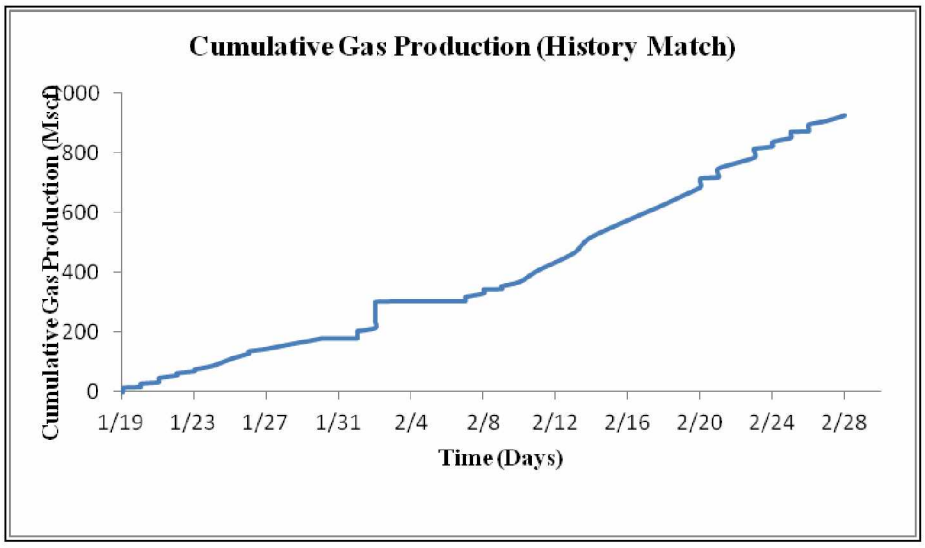

Figure 4.16 CMG STARS cumulative production base case after history match

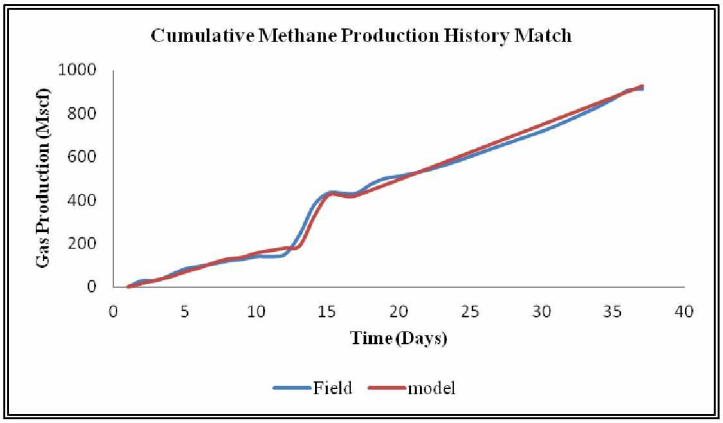

Figure 4.17 Plot comparing field performance with history matched base case model

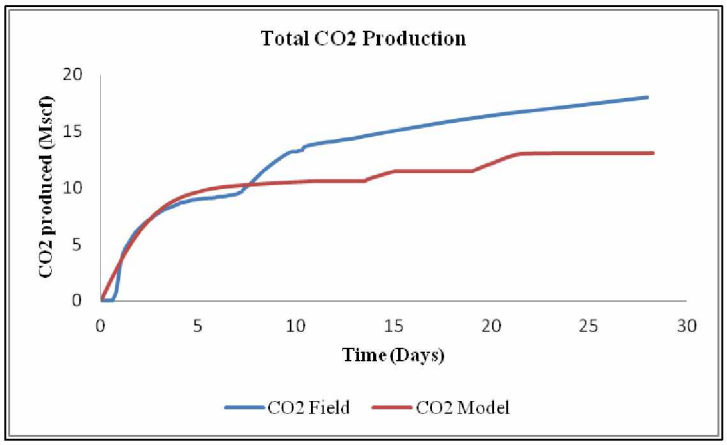

Figure 4.18 Plot comparing produced CO_2 on field with history matched bas case model

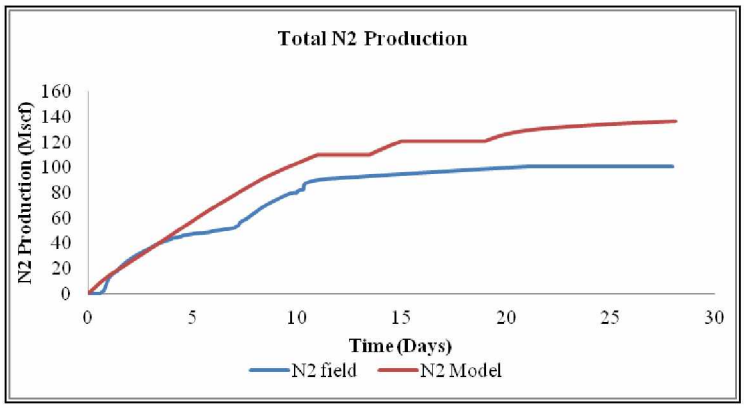

Figure 4.19 Plot comparing produced N_2 on field with history matched bas case model

From the N_2 and CO_2 recovery plots (figures 4.18 and 4.19) it can be observed that the CMG model recovered 25% CO_2 and 68% N_2, whereas, the field recovered 35% CO_2 and more than 50% N_2. There could be multiple factors responsible for gas sequestration in hydrates. The model is considered homogeneous for porosity and permeability distribution, however, the field distribution is heterogeneous. This homogeneity in the model could lead to higher porosity and permeability causing a possible reason for the higher storage of CO_2. In the case of N_2 production the model shows higher recovery compared to the field. During model development, mixed hydrate i.e. CH_4-CO_2-N_2 hydrate formation, is not considered. It is possible that subsurface mixed hydrates are forming causing greater sequestration of N_2 on field compared to model. The CO_2 and N_2 recovery comparison for field and model is shown in figure 4.20.

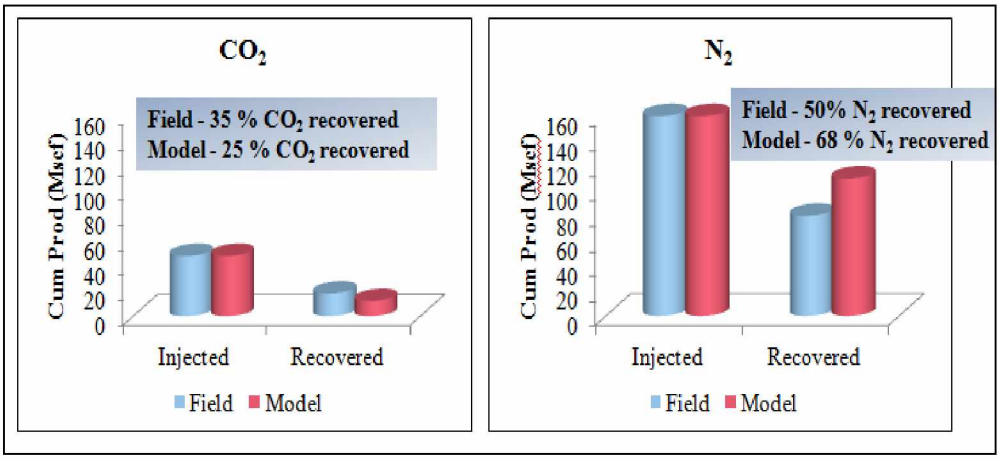

Figure 4.20 CO_2 and N_2 recovery for field and model compared

With the conclusion of the history matching, a temperature profile study was carried out. Figure 4.21 shows the temperature profile at the end of the injection phase for the history matched case. It can be observed here that the

temperature increased near the wellbore that possibly could be the result of formation of CO_2 hydrate which is exothermic in nature. Figure 4.22 shows the average temperature at the end of the production period and states that the overall temperature in the reservoir remained nearly constant. This could be the combined effect of CO_2 hydrate formation (exothermic) followed by CH4 hydrate dissociation (endothermic) which effectively keeps the reservoir temperature nearly constant at 5.5 C (41 F).

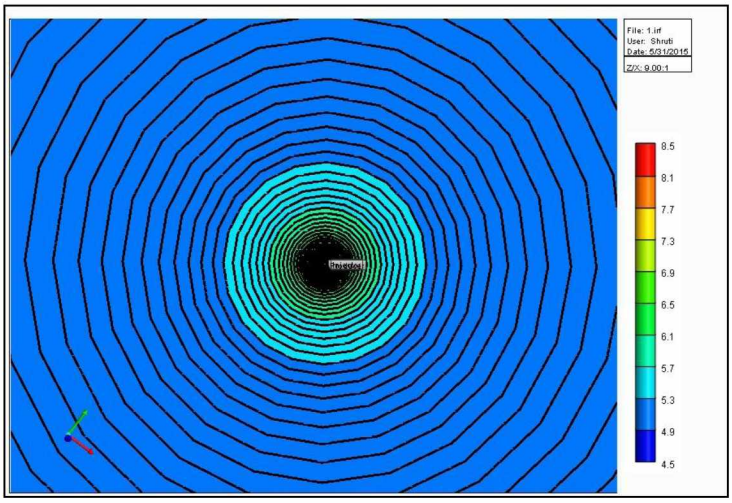

Figure 4.21 CMG STARS Temperature profile at the end of the injection phase for history matched base case

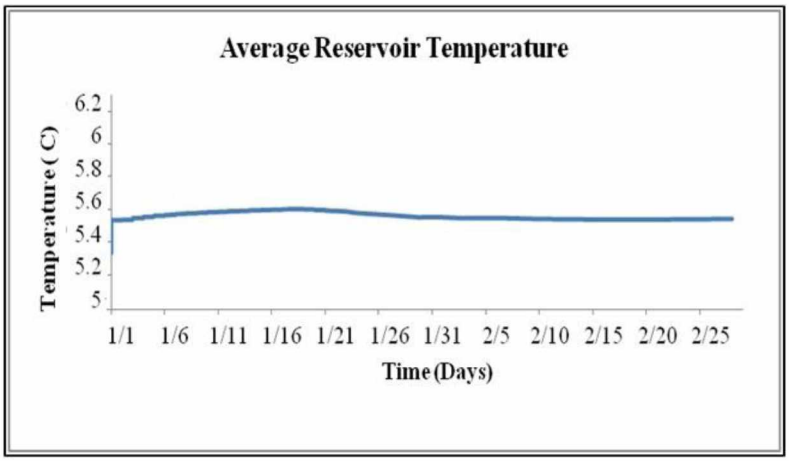

Figure 4.22 History matched base case model average reservoir temperature at the end of production phase

The change in solid concentrations as suggested in the previous section can be seen in Figures 4.23 and 4.24. In these figures, the near wellbore hydrates reacted with injected CO_2 and released methane thereby reducing the solid concentration from 5700 gmole/m3 to almost 3000 gmole/m3.

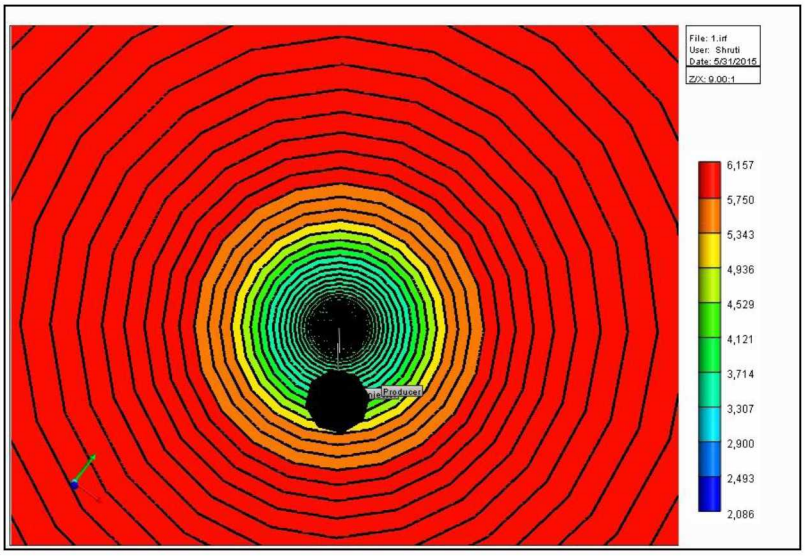

Figure 4.23 Solid phase concentration (methane hydrate) at the end of production phase for history matched base case

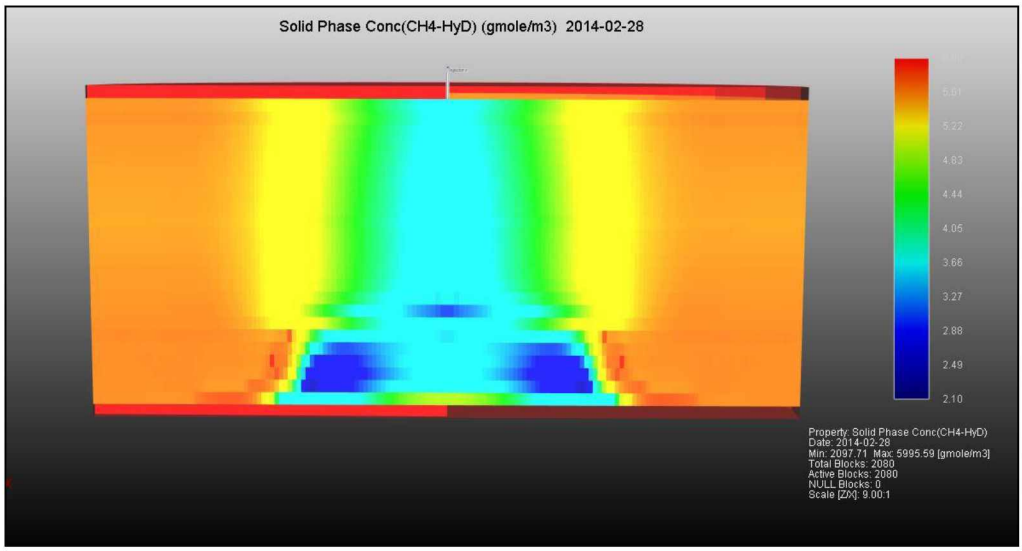

Figure 4.24 Model result showing decrease in hydrate concentration at the end of production phase for history matched base case

4.3 Sensitivity Analysis

The history matched model was used to conduct a sensitivity analysis. The results are explained below. For the sensitivity analysis, four parameters were varied and tested:

1. Hydrate saturation
2. Intrinsic permeability
3. Gas relative permeability
4. Hydrate zone size (introducing free gas zone)

Table 7 Parameters considered for sensitivity analysis

Parameters	Values Varied
Hydrate Saturation	0.5; 0.7; 0.8
Intrinsic Permeability	300; 500; 700; 1000
Relative Permeability	Anderson; Kurihara
Hydrate zone size	675; 673; 680

1. Hydrate Saturation

Figure 4.25 shows the cumulative production plot on varying the hydrate saturation from 0.5 to 0.8. This was done by varying hydrate saturation in terms of the initial solid concentration of the solid hydrate in the reservoir properties. It can be seen from the plot 4.25 that producting increases from 0.5 to 0.7 but decreases for 0.8 hydrate saturation. Since methane hydrate dissociation is an endothermic process, it cools the reservoir. Hence higher hydrate saturation effectively cools the reservoir preventing further hydrate dissociation and causes the fall in gas production (Anderson, 2014).

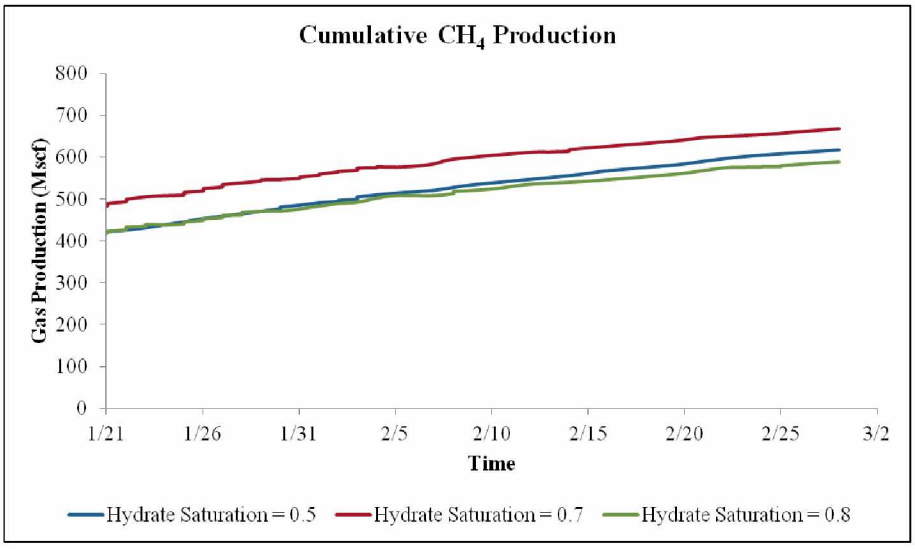

Figure 4.25 Sensitivity analysis on base case for different hydrate saturations

2. Intrinsic Permeability

In tight gas reservoir like the gas hydrates, the reservoir with higher permeability sands drained the reservoir quickly (Figures 4.26 and 4.27). The factors affecting the production could be the combined effect of dissociating hydrates, pressure reduction, and formation of CO_2 hydrate.

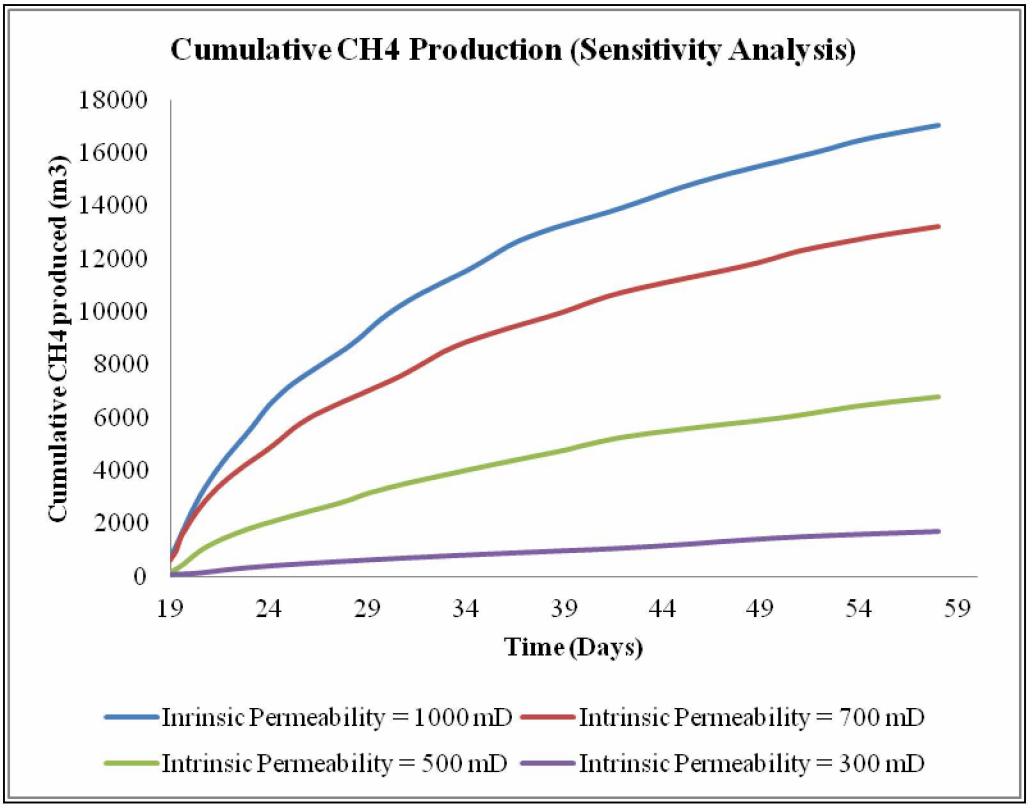

Figure 4.26 Sensitivity analysis on base case showing cumulative production plots for different permeability values

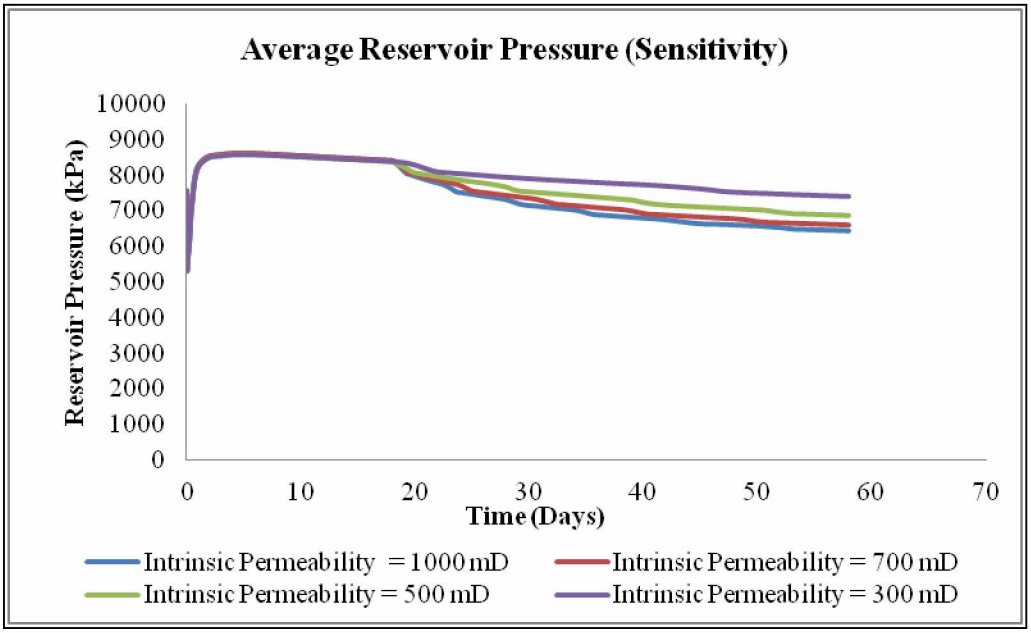

Figure 4.27 Sensitivity analysis on base case showing average pressure for different permeabilities

3. Relative Permeability

Based on the data available, sensitivity analysis was done for two cases of relative permeability values. One model uses the Anderson's relative permeability tables as discussed previously and the second model uses Kurihara relative permeability tables. The most notable difference between the relative permeability curves of Kurihara (2011) and the Anderson relative permeability curves is the gas krg curve. The Kurihara (2011) gas relative permeability curve will result in higher mobility of gas at intermediate water saturations (Figure 4.28) (Blake, 2014).

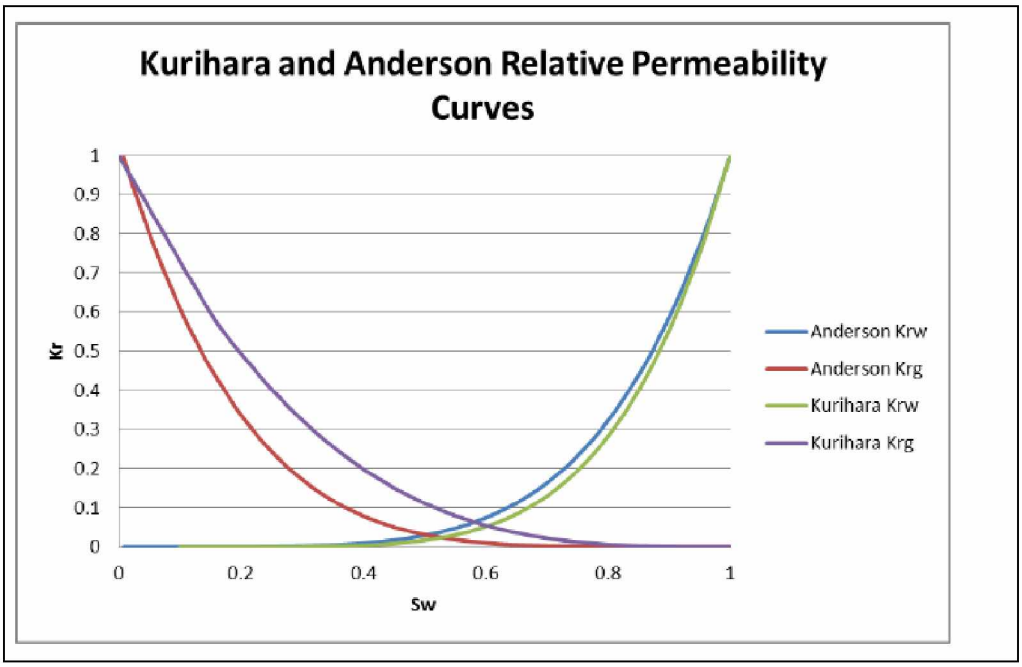

Figure 4.28 Relative permeability curves of Anderson and Kurihara (Blake, 2015)

Figure 4.29 compares production profiles of the Anderson and Kurihara relative permeability curves.

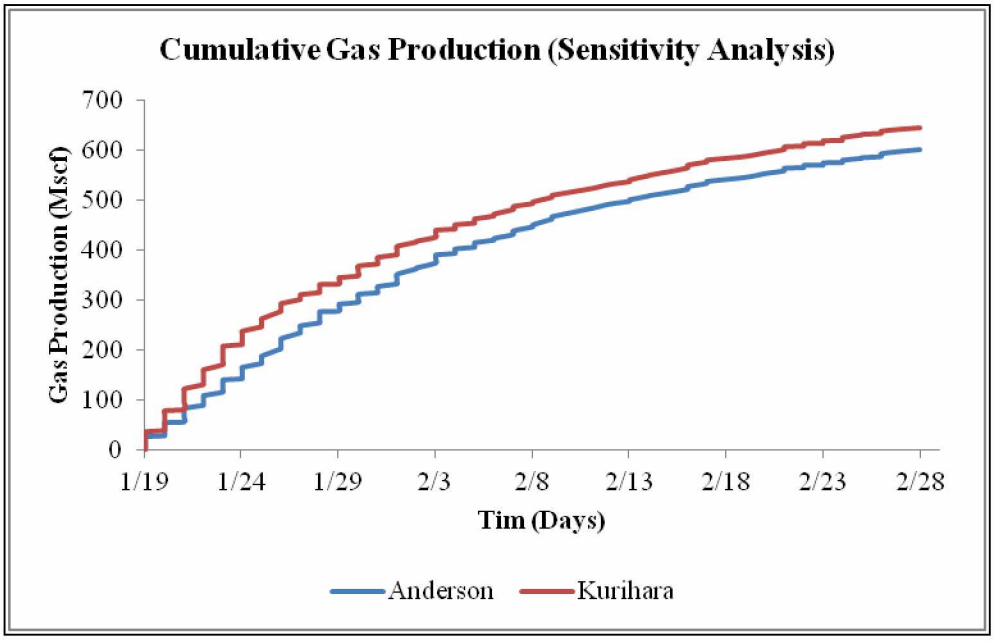

Figure 4.29 Sensitivity Analysis on base case for relative permeability showing cumulative gas production for Anderson and Kurihara relative permeability data

4. Hydrate zone size

CMG-STARS simulation runs were performed by varying hydrate zone size. Figure 4.30 shows cumulative water production with change in hydrate zone size. With decrease in the hydrate zone size and increase in free gas, the water production increased. This could be because gas production reduced the reservoir pressure, resulting in further hydrate dissociation. This increase in the hydrate dissociation could lead to an increase in water production. Figure 4.31 shows that the change in hydrate zone size has a small impact on reservoir pressure, possibly because with decrease in hydrate zone thickness, the gas zone thickness increased, compensating for the loss of the hydrates.

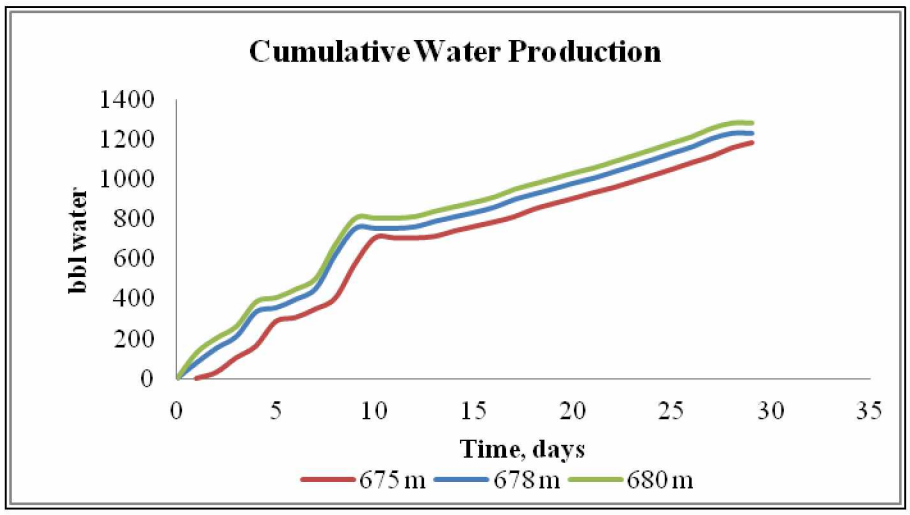

Figure 4.30 Sensitivity Analysis on base case for change in hydrate zone thickness and its effect on water production

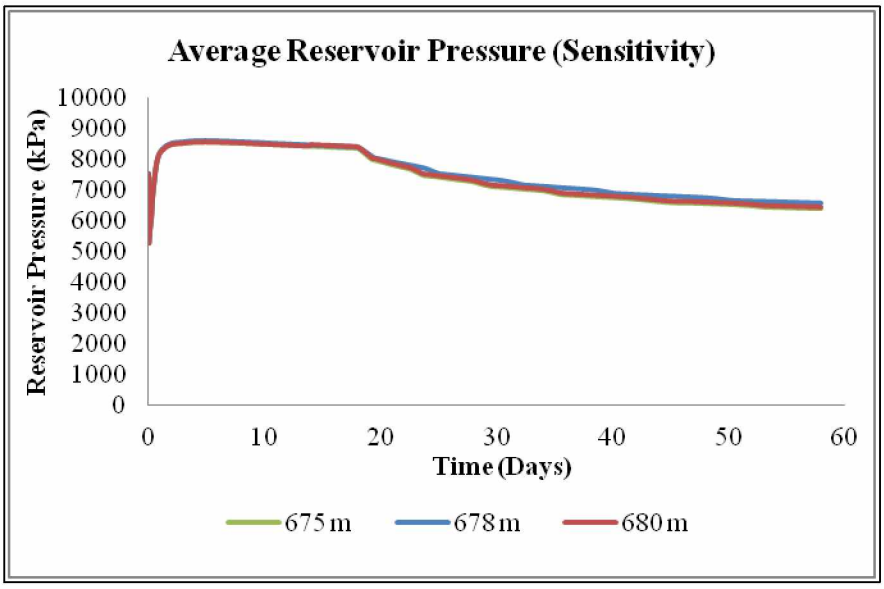

Figure 4.31 Sensitivity Analysis on base case for hydrate zone size and its effect on average reservoir pressure

Figure 4.32 shows the effect of different sensitivity parameters on cumulative gas production. The figure shows the maximum and minimum value obtained during the analysis for each parameter. It can be observed that there is a significant impact of reservoir properties like hydrate saturation, permeability and hydrate zone size on cumulative gas production. Hence it signifies the

importance of accurate reservoir properties during analyzing hydrate reservoirs.

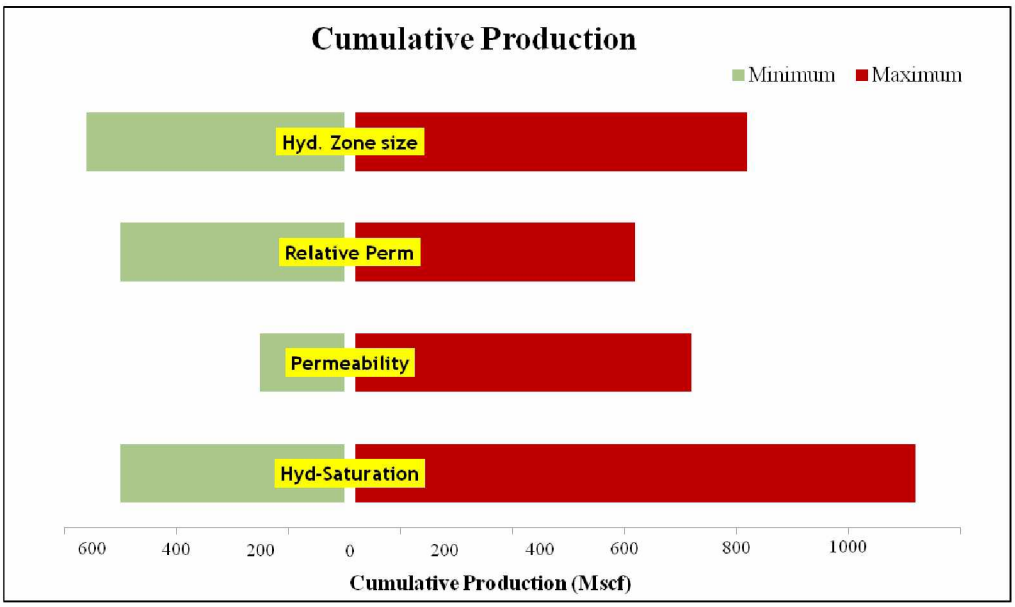

Figure 4.32 Effect of Sensitivity analysis parameters on cumulative gas production. The parameters include hydrate zone size, hydrate saturation, relative permeability and intrinsic permeability.

4.4 Forecasting Study

After the history match and sensitivity analysis, forecasting for the history matched base case was done. During the history match, from the field performance, a sharp drop in BHP from 1200 psi to 200 psi was observed. The original reservoir pressure was about 1080 psi. This difference in the pressures explains that the reservoir needs extra pressure support other than the exchange of CO_2/N_2.

Figure 4.33 shows the production extended for 360 days. It can be observed that the rate of production decreases with time. The cumulative production at the end of one year came out to be around 21000 Mscf. Based on this result it

can be said that the reservoir requires additional pressure support apart from the CO_2 and methane exchange.

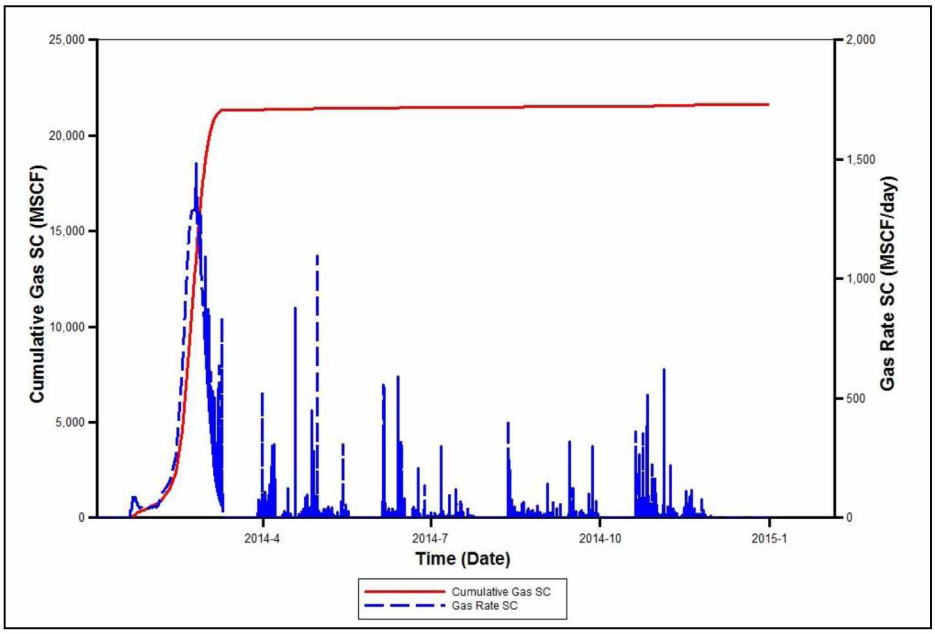

Figure 4.33 Forecast result showing cumulative production and gas rate at the end of 1 year

4.5 Recovery Factor

The calculation of recovery factor was done for the two-month field trial. As stated previously, the reservoir radial extent was assumed to be 2000 ft. Therefore, any change in the reservoir volume could change the recovery factor. For the current scenario, the original gas in place in the form of hydrate was equal to $9\,x\,10^5$ bscf, which was a high value because of the huge reservoir size assumed. The cumulative gas produced was 900 mscf as per the history match results. Hence, the recovery factor for the field test model in which production lasted nearly 40 days came out to be 0.00003%. In the case of long term production of one year, the cumulative production was 21900 mscf and the recovery factor was 0.0008%.

Chapter 5 Conclusion

CMG STARS has been successful in modeling the guest molecule exchange process for recovering CH_4 gas from hydrates on injecting a mixture of CO_2 and N_2.

The simulation results conclude that CO_2-CH_4 exchange takes place for long term production of 1 year however it doesn't seem to be feasible due to pressure decline in the reservoir and the absence of any secondary pressure support.

The sensitivity analysis of the reservoir properties show that accurate field data about reservoir properties can have a significant effect on the cumulative production. Since the entire process is controlled by the exothermic and endothermic reactions taking place due to exchange of guest molecules, reservoir temperature is an important parameter that needs to be monitored.

Not considering mixed hydrate formation in this modeling work doesn't have any effect on the CH_4 recovery however the N_2 recovery is lower when compared to field data after history match. This shows that consideration of mixed hydrate formation in modeling could be a significant factor in ensuring the accuracy of the history match.

Chapter 6 References

Brian Anderson, Ray Boswell, Timothy S. Collett, Helen Farrell, Satoshi Ohtsuki, Mark White and Margarita Zyrianova, *Review of the Findings of the Ignik Sikumi CO_2-CH_4 Gas Hydrate Exchange Field Trial*, presented at the 8th International Conference on Gas Hydrates (ICGH8-2014), Beijing, China, 28 July01 August, 2014.

Dallimore, S. R. and Collett, T. S. *Scientific Results from the Mallik 2002 Gas Hydrate Production Research Well Program, Mackenzie Delta, Northwest Territories, Canada.* Geological Survey of Canada Bulletin, No. 585, 140 p, 2005.

Darvish, M. P.*Gas Production from Hydrate Reservoir and Its Modeling.* Journal of Petroleum Technology (JPT), pp. 65-71, June 2004.

David Schoderbek, Kenneth Lloyd Martin, James Howard, Suntichi Silngarmlert, and Keith Hester, *North Slope Hydrate Field trial: CO_2/CH_4 Exchange*, OTC 23725, presented at the Arctic Technology Conference, Houston, Texas, 3-5 December, 2012.

Gaddipati, M. , *Reservoirs Modeling of Gas Hydrate Deposits in North Slope Alaska and Gulf of Mexico*, PhD thesis, West Virginia University, Morgantown, West Virginia, 2014.

Ganti, G. *The Effects of Permeability and Well Completion on Methane Gas Production from Hydrate-Bearing Reservoir*. M. S. Thesis, The University of West Virginia, Morgantown, West Virginia, 76p, 2007.

George J. Moridis, Timothy S. Collett, Ray Boswell, M. Kurihara, Matthew T. Reagan, Carolyn Koh and E. Dendy Sloan, *Towards Production from Gas Hydrates: Current Status, ASSESSMENT OF Resources, and Simulation-Based Evaluation of Technology and Potential*, SPE 114163, presented at the SP Unconventional Reservoirs Conference, Keystone, Colorado, 10-12 February, 2008.

Hall, K.R. and Yarborough, L. *A New Equation of State for Z-Factor Calculations*. Oil & Gas J. 71 (25): 82, 1973.

Hammerschidt, E. G. Ind. Eng. Chem., 26, 851, 1934.

Hauge L. P., Birkedal K. A., Ersland G. & Graue A., *Methane Production from Natural Gas Hydrates by CO_2 Replacement Review of Lab Experiments and Field Trial*, SPE paper 169198-MS, presented at Bergen, Norway, April 2, 2014.

I. Rao, L. E. Zerpa, E. D. Sloan, C. A. Koh , A. K. Sum and T. J. Danielson, *Multiphase Flow Modeling of Gas-Water-Hydrate System*, OTC 24099, presented at the Offshore Technology Conference, Houston, Texas, 6-9 May, 2013.

Jennifer Blake, *Analysis of Alaska North Slope Hydrate-Bearing Reservoir Through Simulation to Demonstrate Technical Feasibility of Gas Production with Sensitivities on Production Development Schemes*, MS research, University of Alaska Fairbanks, 2015.

Katz, D. L., *Prediction of Conditions for Hydrate Formation in Natural Gases*. Trans. pp. 140-160, AIME, 1945.

Kurihara, M., Sato, A., Funatsu, K. et al. *Analysis of Formation Pressure Test in the Mount Elbert Methane Hydrate Reservoir through Numerical Simulation*. Journal of Marine and Petroleum Geology **28** (2): 502-516, 2011.

Mark White &Won Suk Lee, *Guest Molecule Kinetics for the 2012 Ignik Sikumi Gas Hydrate Field Trial*, OTC-25374-MS, presented at the Offshore Technology Conference, Houston, Texas, 5-8 May, 2014.

Max, D., *Natural Gas Hydrate in Oceanic and Permafrost Environments*, Kluwer Academic Publishers, Dordrecht, Netherlands, 2000.

Mc Mullan, R.K., Jeffrey,GA., J. Chem. Phys., 42, 2725, 1965.

Moridis, et al., Toward Production From Gas Hydrates: *Current Status, Assessment of Resources, and Simulation-Based Evaluation of Technology and Potential*. SPE Reservoir Evaluation & Engineering, Vol. 12, 745-771, 2009.

NETL, C. P. 2012 ConocoPhillips, Gas Hydrates Production Test, Progress Report Second HALF, 2011.

NETL, C. P. 2013 ConocoPhillips Gas Hydrate Production Test, Final Technical Report, 2013.

Ripmeester, J. A., Tse, J. S, Ratcliffe, C. I., and Powell, B. M. : *A New Clathrate Hydrate Structure*, Nature, 325, 135, 1987.

Sloan, E.D.; Koh, C. A. Clathrate hydrates of natural gases, 3rd ed, p-70, 2007.

Stillinger, Water Revisited. Vol. 209, 8, 1980.

Stone, H. L. *Estimation of Three-Phase Relative Permeability and Residual Oil Data*. Journal of Canadian Petroleum Technology, Vol. 12, No. 4, pp. 53-61, 1973.

Swinkles, W. J. A. M. and Drenth, R. J. J. *Thermal Reservoir Simulation Model of Production from Naturally Occurring Gas Hydrate Accumulations*. SPE Reservoir Evaluation and Engineering, Vol. 3, No. 6, December 2000.

Timothy S. Collett, *Gas Hydrate Reservoir Properties*, SPE 168760, presented at Unconventional Resources Technology Conference, Denver, Colorado, 12-14 August, 2013.

Timothy J. Kneafsey and George J. Moridis, *Methane Hydrate Dissociation by Depressurization in a Mount Elbert Sandstone Sample: Experimental Observations and Numerical Simulations*, OTC 22150, presented at the Arctic Technology Conference, Houston, 7-9 February, 2011.

U. S. Energy Information Administration, Annual Energy Outlook, 2015.

Yousif, M. H. and Sloan, E. D. *Experimental Investigation of Hydrate Formation and Dissociation in Consolidated Porous Media*. SPE Reservoir Engineering, November 1991, pp. 452-458.

Appendix A . Thermal and Fluid Component Properties

A1. Thermal Properties

Table A1 summarizes the properties of rock and fluids initialized for the Ignik Sikumi well.

Description	**CMG-STARS Keyword**	**Value SI units**	**Value Field units**
Reservoir rock type	*ROCKTYPE	1	1
Vol Heat Capacity (rock)	*ROCKCP	8.00E+5 J/(m3*C)	
Thermal Heat Conductivity			
Reservoir Rock	*THCONR	1.50E+05 J/(m*day*C)	
Solid phase/hydrate	*THCONO	3.93E+04 J/(m*day*C)	
Water	*THCONW	6.00E+04 J/(m*day*C)	
Gas	*THCONG	2.93E+03 J/(m*day*C)	
Phase Mixing	*THCONMIX	COMPLEX	

A2. Fluid Component Properties

Table A2 summarizes the fluid component properties initialized for the Ignik Sikumi#1 well.

Property	**CMG-STARS Keyword**	**Value SI unit**
Component	*COMPNAME	WATER/CH4/CO2/N2/CH4HYDRATE/ CO_2Hydrate
Molecular weight (kg/kg-mole)	*CMM	18.015e-3/16.043e-3/0.04401/28.013e-3/119.543e-3/182.6E-3
Critical Pressure (kPa)	*PRCIT	0/4.600E+3/7376/3399/
Critical Temperature (C)	*TCRIT	0/-8.255E+1/31.05/-147
Molar density (liquid) gmole/m3	*MOLDEN	55501.5/NA/NA/NA/NA/NA
Liquid Phase Viscosity (cp)	*AVISC *BVG	0/ NA/NA/NA/NA/NA 0/ NA/NA/NA/NA/NA
Gas Phase Viscosity (Using correlation) cp/C	*AVG *BVG	0/ 3.8E-3/ 3.8E-3/ 0/NA/NA 0/0/0/0/NA/NA
Liq Compressibility (1/kPa)	*CP	0/ NA/NA/NA/NA/NA

Coefficient of thermal expansion First coefficient (1/C) Second coefficient (1/(C*C))	 *CT1 *CT2	 0/ NA/NA/NA/NA/NA 0/ NA/NA/NA/NA/NA
Heat capacity in the liquid phase	*CPL1 (J/(gmole*C) *CPL2 (J/(gmole*C*C) *CPL3 (J/(gmole*C*C*C) *CPL4 (J/(gmole*C*C*C*C)	0/0/0/0/NA/NA 0/0/0/0/NA/NA 0/0/0/0/NA/NA 0/0/0/0/NA/NA
Heat capacity in the gas phase	*CPL1 (J/(gmole*C) *CPL2 (J/(gmole*C*C) *CPL3 (J/(gmole*C*C*C) *CPL4 (J/(gmole*C*C*C*C)	0/1.9251E+1/1.9795E+1/0/NA/NA 0/5.213E-2/7.344E-2/0/NA/NA 0/1.197E-5/5.602E-5/0/NA/NA 0/-1.132E-8/1.715E-8/0/NA/NA
Reaction Stoichiometry	*STOREAC	1/0/0/0/1/0
Product Stoichiometry	*STOPROD	6.75/1/0/0/0/0
Component reaction order	*RORDER	1/0/0/0/1/0
Reaction frequency factor	*FREQFAC	1.097058E+13

Reaction enthalpy (J/gmole)	*RENTH	-51857.9364
Activation energy (J/gmole)	*EACT	89660.02503

Appendix B. Tubing Tables

B1. Injection tubing table

INJECTOR	Flow Rate	WHP Well Head Pressure	WHP
	m3/day	KPa	Psig
1	1132.672	8835.83	1281.53
2	1699.008	8746.75	1268.61
3	1415.84	8798.60	1276.13
4	707.92	8820.94	1279.37
5	2265.344	8830.94	1280.82
6	1415.84	8832.59	1281.06
7	1415.84	8798.67	1276.14
8	1132.672	8852.24	1283.91
9	1132.672	8737.45	1267.26
10	1132.672	8842.38	1282.48
11	1415.84	8799.91	1276.32
12	1415.84	8850.45	1283.65
13	1415.84	8693.39	1260.87
14	1415.84	6894.75	1189.73

B2. Production tubing table

PRODUCTION	Flow rate	GOR	WHP	WHP
	m3/day	m3/m3	KPa	psig
1	0	0	1505.95	218.42
2	815.3278	0	1873.30	271.7
3	0	0	1252.98	181.73
4	764.2193	0	1598.61	231.86
5	754.8472	0	1193.20	173.06
6	344.7098	0	950.44	137.85
7	339.9993	0	44.88	6.51
8	373.5115	0	0	0
9	211.6341	0	966.36	140.16
10	351.8438	0	953.68	138.32
11	0	0	872.11	126.49
12	334.3206	0	637.42	92.45
13	2548.483	0	22.47	3.26
14	3812.463	0	0	0
15	1587.377	0	0	0
16	1.239466	0	0	0

17	0	0	1879.85	272.65
18	1172.401	0	1224.78	177.64
19	767.4241	0	1420.04	205.96
20	292.4682	0	1398.11	202.78
21	370.7058	0	1297.17	188.14
22	452.0551	0	1132.67	164.28
23	531.8921	0	1114.26	161.61
24	596.3063	0	1098.95	159.39
25	664.2208	0	1102.88	159.96
26	664.1976	0	1108.74	160.81
27	660.6635	0	1086.47	157.58
28	652.5468	0	1086.61	157.6
29	645.27	0	1095.71	158.92
30	658.3918	0	1187.20	172.19
31	750.7095	0	1200.85	174.17
32	812.5942	0	1300.00	188.55
33	849.596	0	1289.59	187.04
34	869.9207	0	215.18	31.21
35	980.7919	0	212.63	30.84
36	1082.351	0	68.94	10
37	185.4783	0	4.82	0.7